Title

THE FORMATION OF BARIUM TITANATE CERAMICS BY SOLID STATE REACTION

Author

Bierach, J.W.

Publication Date

1989-05-05

Thesis/dissertation

LBL-26519

Lawrence Berkeley Laboratory

UNIVERSITY OF CALIFORNIA

Materials & Chemical Sciences Division

The Formation of Barium Titanate Ceramics by Solid State Reaction

J.W. Bierach
(M.S. Thesis)

May 1988

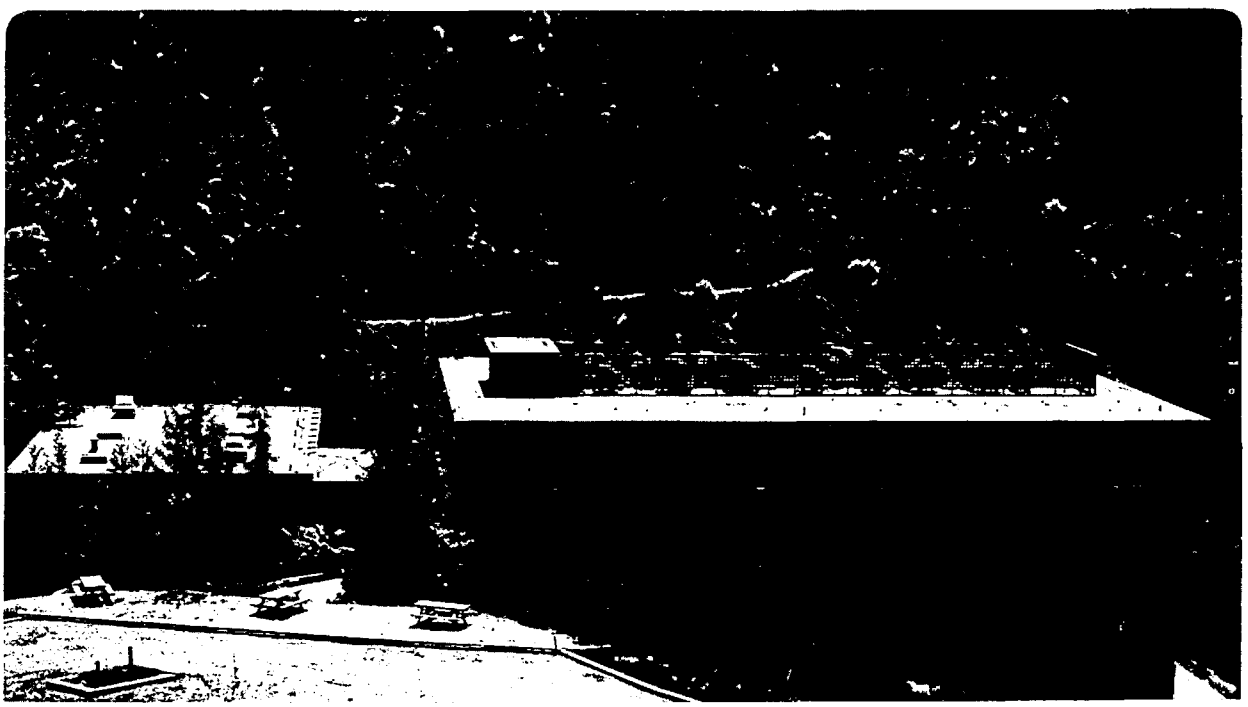

Prepared for the U.S. Department of Energy under Contract Number DE-AC03-76SF00098.

DISCLAIMER

LBL-26519

THE FORMATION OF BARIUM TITANATE CERAMICS BY SOLID STATE REACTION

Jeff W. Bierach
(M.S. Thesis)

Materials and Chemical Sciences Division
Lawrence Berkeley Laboratory
and Department of Materials Science and Mineral Engineering
University of California
Berkeley, California 94720

May 1988

This work was supported by the Director, Office of Energy Research, Office of Basic Energy Science, Materials Sciences Division of the U.S. Department of Energy under Contract Number DE-AC03-76SF00098.

Table of Contents

List of Tables

List of Figures

Acknowledgements

I would like to express my gratitude to Professor Alan W. Searcy for his guidance, support, and patience throughout this work, and for his help in revising this manuscript.

I would like to thank Professors Neil Bartlett and Lutgard C. DeJonghe for their helpful comments regarding this work.

I also wish to thank Dr. David J. Meschi for all of our conversations and for his help in all matters of science.

I am grateful to Professor Jeffrey A. Reimer for his help and guidance throughout my studies.

I am also grateful to my parents for their support and for raising me in an environment which made it possible for me to come to Berkeley.

To my wife Carol, I give my greatest thanks for being so supportive and understanding, and for being such a wonderful mother to Rachel and Katherine.

1 Introduction

Barium titanate ceramics have been widely investigated for many years because they have interesting and technically important properties. Perovskite type $BaTiO_3$ exhibits a positive temperature coefficient of resistivity, and is a piezoelectric ceramic. $Ba_2Ti_9O_{20}$ exhibits useful properties for a microwave frequency dielectric[1].

The formation of these and other barium titanate ceramics by solid state reaction between $BaCO_3$ and TiO_2 is believed to be diffusion controlled and to proceed by the following reaction steps[2,3,4,5,6]: $BaTiO_3$ is formed first at the TiO_2 - $BaCO_3$ interface, with the diffusion of "BaO" into the TiO_2 accompanied by the evolution of CO_2 from the decomposition of $BaCO_3$. After the initial layer of $BaTiO_3$ is formed, Ba_2TiO_4 forms at the $BaTiO_3$ - $BaCO_3$ interface, while $BaTiO_3$ advances into the TiO_2 by diffusion of "BaO" through the outer Ba_2TiO_4 and $BaTiO_3$ to the TiO_2 - $BaTiO_3$ interface (Figure 1a). When the $BaCO_3$ is all reacted, the outer Ba_2TiO_4 decomposes into $BaTiO_3$ with the diffusion of "BaO" through the inner $BaTiO_3$ where reaction with the remaining TiO_2 takes place to form $BaTiO_3$.

The above reaction steps are oversimplified in terms of the nature of the diffusing species and of secondary phase formation. The quotation marks placed around BaO indicate that the nature of the diffusing species is unknown. If electrical neutrality is to be retained, the diffusion of Ba through $BaTiO_3$ and other product layers to react with TiO_2 must be accompanied by O diffusion or by a counter current of Ti. Diffusivities of Ba, Ti, and O in these ternary oxides are not known. The lattice diffusivity of Ba in rutile at 1070°C is $D_{Ba} \approx 2 \times 10^{-9}$ cm^2/s compared to $D_{Ti} \approx 10^{-11}$ cm^2/s and $D_O \approx 10^{-13}$ cm^2/s for self diffusion of Ti and O in rutile[7]. Experimental work by Nakayama and Sasaki[8] has confirmed that Ba diffuses into rutile. Because the diffusivity of Ti is higher than that of O in TiO_2, and because the volume change is large (200%) when TiO_2 is converted to $BaTiO_3$, it seems likely that Ba ion diffusion through the ternary oxides is countered by Ti ion diffusion in the reverse direction in the ratio of $2Ba^{+2} : Ti^{+4}$ to maintain electrical neutrality. However, the possibility of Ba diffusion coupled by oxygen diffusion cannot be ruled out without experimental evidence.

This work addresses a different aspect of the analyses of the $BaTiO_3$ formation reaction will. The occurrence of titanate phases other than $BaTiO_3$ and Ba_2TiO_4 in the reaction of $BaCO_3$ and TiO_2 has been reported[2,3,4,9,10], but except in the study of Templeton and Pask[4] no systematic interpretation of these results has been formulated. The presence of secondary phases is usually attributed to such causes as insufficient mixing or other preparative factors[11], and in some cases the secondary phase is not even identified[5b]. It will be shown in this work that the occurrence of additional titanate phases during the course of the reaction is to be expected.

1.1 Heterogeneous Solid State Reactions

The formation of $BaTiO_3$ in the solid state is a heterogeneous reaction, meaning that the reactants become separated by phase boundaries and reaction products as soon as any product phase has formed. For the reaction to proceed, it is necessary for diffusion to occur across phase boundaries and intermediate phases, the driving force being the activity gradients between the two end members. For the $BaCO_3$ - TiO_2 reaction couple, the initial activity of TiO_2 decreases from unity on the TiO_2-side to zero on the $BaCO_3$-side of the boundary. This variation is shown schematically in Figure 1a for the reaction sequence described, as often assumed[5,6,11,12,13,14], if Ba_2TiO_4 is the only intermediate reaction product present during $BaTiO_3$ formation. Figure 1b shows schematically the activity variation expected from the BaO - TiO_2 phase diagram.

The BaO-TiO_2 phase diagram (Figure 2) shows that there are four equilibrium phases between the compositions $BaTiO_3$ and TiO_2. It is possible that any of these phases might be formed between $BaTiO_3$ and TiO_2 during the course of solid state reaction if local thermodynamic equilibrium is approached. Figure 1b is a modification of Figure 1a where all of the possible intermediate phases, except those that have been reported[15,16,17,18,19] to be thermodynamically unstable ($BaTi_5O_{11}$, $BaTi_6O_{13}$, and $BaTi_2O_5$) have been included between the reactants $BaCO_3$ and TiO_2.

Although any of the phases shown in Figure 1b might form, there are kinetic factors which could keep them from forming. A nucleation barrier could prevent a phase from forming. Some of the phases might only be formed transiently in a poorly

crystallized state or in such small amounts that detection would be difficult. If relatively thin inner layers of product phases are surrounded by a thick outer product layer, the inner phases could go undetected by the typical methods of characterization such as x-ray diffraction, optical microscopy, and scanning electron microscopy.

In both Figures 1a and 1b, the relative thicknesses of the various phases are not drawn to scale. In fact, the thickness of each phase depends inversely on the rate of diffusion through that phase[20]. Thus, if diffusion through a phase is rapid, it will form a relatively thin layer. If diffusion through a phase is slow, its layer will be relatively thick. A thin inner product phase surrounded by a thick layer of another phases or phases, as depicted in Figure 3 may be present. Such a circumstance could explain why many of the possible intermediate phases have not been observed.

If some of the stable intermediate phases do fail to nucleate, other barium titanates that are unstable at the temperature of study but which are easier to nucleate may be present during reaction. It is worthwhile, therefore, to seek evidence of the presence or absence of $BaTi_5O_{11}$, $BaTi_6O_{13}$, and $BaTi_2O_5$ which are not stable at the temperature of study of the reaction, but which have been reported to form at other temperatures.

1.2 Observed Intermediate Reaction Products

In this section, the various barium titanate phases which might be formed during solid state reaction will be discussed. There are six equilibrium phases between BaO and TiO_2 on the phase diagram (Figure 2), as well as the three metastable phases mentioned above. A number of these phases have been observed during the course of solid state reaction. Other phases which have been reported to exist are mentioned in section 1.2.10, but these phases are not expected to be found in this work.

1.2.1 Ba_2TiO_4 - Equilibrium Phase

Barium orthotitanate, Ba_2TiO_4, which has been widely reported, is formed between the reactant $BaCO_3$ and initial product $BaTiO_3$ during the reaction of $BaCO_3$ and

TiO_2[2-6]. The phase is easy to detect and its presence has an undesirable effect on the electrical properties of $BaTiO_3$ ceramics[11]. Templeton and Pask[4] have shown that the formation of Ba_2TiO_4 can be suppressed below 1100°C in one atmosphere of CO_2.

1.2.2 $BaTiO_3$ - Equilibrium Phase

$BaTiO_3$ is the phase of most technological interest in the BaO - TiO_2 system. It is typically formed by solid state reaction between $BaCO_3$ and TiO_2 as described in the introduction. Many authors[2-6,9-11,13,14,21,22,23] have studied this reaction in an effort to determine the affect of particle size, mixing, atmosphere, and reaction temperature on the microstructure and electrical properties of sintered $BaTiO_3$ ceramics.

1.2.3 $Ba_6Ti_{17}O_{40}$ - Equilibrium Phase

This phase has not been reported to form as an intermediate reaction product. It is has been prepared[24] by quenching partially melted samples of composition $BaCO_3$: TiO_2 = 1 : 3 from 1400°C, and it has also been prepared[24] by slowly cooling samples of composition 1 : 2.5 after heating at 1400°C. Negas, et. al.[25], are the only authors to report the formation of $Ba_6Ti_{17}O_{40}$ by solid state reaction. They observed $Ba_6Ti_{17}O_{40}$ after reaction below 1300°C in mixtures which ranged in composition from $1BaCO_3 : 2TiO_2$ to $1BaCO_3 : 3TiO_2$. $Ba_6Ti_{17}O_{40}$ was determined to exist as an equilibrium phase down to 800°C by slowly cooling samples from 1300°C and quenching from 800°C.

1.2.4 $Ba_4Ti_{13}O_{30}$ - Equilibrium Phase

A phase previously reported in the earlier literature as $BaTi_3O_7$, now known to be $Ba_4Ti_{13}O_{30}$[26], has been reported by many authors to be present in small amounts during the reaction of $BaCO_3$ and TiO_2 to form $BaTiO_3$[2,3,4,9,22]. This phase forms readily by solid state reaction.

1.2.5 $BaTi_4O_9$ - Equilibrium Phase

Templeton and Pask reported very small amounts (≈1 mole %) of $BaTi_4O_9$ during the intermediate stages of reaction in $BaCO_3$-TiO_2 mixtures. Rase and Roy[27] prepared

$BaTi_4O_9$ "very easily" by solid state reaction below 1400°C of a mixture of composition $BaO : TiO_2 = 1 : 4$. In studies of the formation of $Ba_2Ti_9O_{20}$ from TiO_2 and $BaTiO_3$, O'Bryan and Thomson[28] observed $BaTi_4O_9$ as a second phase in the majority of their samples. $BaTi_4O_9$ has also been found to form at exposed surfaces of Ba-doped rutile ceramics heated under various conditions[7,29].

1.2.6 $Ba_2Ti_9O_{20}$ - Equilibrium Phase

This phase has not been reported to form as an intermediate reaction product during reaction of $BaCO_3$ and TiO_2. O'Bryan and Thomson prepared $Ba_2Ti_9O_{20}$ from mixtures of $BaTiO_3$ and TiO_2 which were pre-fired in O_2 at 1350-1400°C for 6 hours, and then equilibrated for 12 hours in O_2 at temperatures between 1100°C and 1400°C.

1.2.7 $BaTi_5O_{11}$ - Metastable Phase

In mixtures of $BaCO_3 : TiO_2 = 1 : 4.5$ and $1 : 5$ heated at 1100°C, O'Bryan and Thomson observed several weak diffraction lines of this phase along with those of $BaTi_4O_9$ and TiO_2[15]. When the composition $BaO : TiO_2 = 1 : 5$ was prepared from an aqueous solution of $Ba(NO_3)_2$ + $Ti(OC_3H_7)_4$ and prereacted at 1000°C for 2 hours, $BaTi_5O_{11}$ formed as the major phase. Tillmans[16] found crystals of $BaTi_5O_{11}$ in samples of composition $BaO : TiO_2 = 1 : 4$ which were melted and quenched from 1400° to 1500°C.

1.2.8 $BaTi_6O_{13}$ - Metastable Phase

The only evidence for the formation of this phase is by Tillmanns[17], who formed $BaTi_6O_{13}$ when a mixture of composition $BaO : TiO_2 = 1 : 4$ was melted and quenched from 1460°C. For the compositions $BaCO_3 : TiO_2 = 1 : 4.5$ and $1 : 5$ heated at 1100°C, O'Bryan and Thomson[15] identified only $BaTi_4O_9$ and $BaTi_5O_{11}$ by x-ray powder diffraction. $BaTi_6O_{13}$ is not expected to be found in the present study.

1.2.9 $BaTi_2O_5$ - Metastable Phase

Several authors have reported the formation of this phase from samples of composition between 60 and 78 mole % TiO_2 which were cooled from a

melt[18,19,25,27]. O'Bryan and Thomson[18] and Jonker and Kwestroo[19] have shown that $BaTi_2O_5$ is unstable at temperatures below 1312°C, and that this phase is not an equilibrium phase. Jonker and Kwestroo, and Negas et. al.[25], were unable to form this phase by solid state reaction. Therefore, the phase is not expected to be found in the present study at 1050°C.

1.2.10 Other Phases

It is believed that the list above includes all characterized phases of the BaO - TiO_2 system, and the structures of all of these phases are known. Several authors report the presence of unidentified phases which could be any of the above or some other phases such as the ones mentioned below.

Other phases which have been reported in the literature include those which have been named incorrectly, and others which are structurally similar to the barium titanates but exhibit chemical variations or contain other elements[30]. Phases reported as $Ba_2Ti_3O_8$, $BaTi_3O_7$ and $Ba_2Ti_5O_{12}$ are probably $BaTiO_3$, $Ba_4Ti_{13}O_{30}$ and $Ba_6Ti_{17}O_{40}$, respectively[19,25,30]. In the chemically variant phases, the Ti^{+4} ion can be partially substituted by Ti^{+3} ($Ba_2Ti_2^{3+}Ti_4^{4+}O_{13}$) or by a vacancy ($Ba_2Ti_{5.5}O_{13}$). The Ti^{+4} ion can also be partially substituted by Al^{+3} ($Ba_4Ti_{10}Al_2O_{27}$) and Pt^{+4} ($Ba_4[Ti,Pt]O_3$ and $Ba_4[Ti,Pt]_2PtO_{10}$),

2 Objective

The objective of the current research project is to investigate the existence of secondary phases between the reactants BaO and TiO_2 during the formation of barium titanate ceramics. It was stated earlier that $BaTiO_3$ is the first phase observed in the reaction of $BaCO_3$ and TiO_2, and only one phase (Ba_2TiO_4) has been detected on the BaO-rich side of $BaTiO_3$. To study the phases which form on the TiO_2-rich side of $BaTiO_3$, it is not necessary to start with $BaCO_3$ and TiO_2--it is sufficient to study the system $BaTiO_3$ - TiO_2. This simplification is valid because any solid state reaction, no matter how complex, can be broken down into interactions between pairs of solid phases. The use of $BaTiO_3$ and TiO_2 as reactants simplifies the problem of phase identification by eliminating two phases, $BaCO_3$ and Ba_2TiO_4, and it also eliminates problems with controlling extraneous reactions when these two phases are present. Mixtures of $BaCO_3$ and TiO_2 are highly reactive with common crucible materials such as Al_2O_3 and platinum. Mixtures of $BaTiO_3$ and TiO_2 can be fired at moderate temperatures (1100°C) in a platinum basket with little or no reaction with the platinum.

The reaction between $BaTiO_3$ and TiO_2 was studied at 1050°C. This temperature was selected because it was near temperatures used in earlier work in the literature[4] and because, when produced for practical applications, barium titanate ceramics are often pre-reacted at 1050-1100°C before being fired at temperatures greater than 1300°C. The compositions and relative amounts of phases formed as a function of time at 1050°C were identified by x-ray diffraction. The method of analysis increases the sensitivity with which phases can be detected over those of past studies, but it is emphasized that absence of x-ray diffraction evidence does not prove that a phase has not formed; the phase might be present in an amount below the detection limit for that phase.

3 Quantitative Analysis by X-ray Diffraction

3.1 General Principles

Quantitative analysis by x-ray diffraction is based on the principle that the intensity of any diffraction peak of a particular phase in a mixture depends on the concentration of that phase in the mixture. The method used for quantitative analysis is the "matrix-flushing" technique developed by Chung[31] and is an extension of the internal standard method of Klug and Alexander[32]. An outline of the theory will be given below. The intensity equation for x-ray powder diffraction is

$$I_{hkl} = \left[\frac{I_o e^4 \lambda^3 d}{32\pi m^2 c^4 r}\right]\left[\frac{1+\cos^2 2\theta}{\sin^2\theta\cos\theta}\right]\left[N^2 F^2 p e^{-2M}\right]\frac{V}{2\mu} \qquad (1)$$

I_{hkl} = intensity of x-rays diffracted by the *hkl* plane
I_o = intensity of primary x-rays beam
e = electron charge
m = electron mass
λ = wavelength of x-rays
d = slit width of detector
c = velocity of light
r = radius of diffractometer circle
θ = Bragg angle
N = number of unit cells per unit volume
p = multiplicity factor
e^{-2M} = temperature factor
F = structure factor
μ = linear absorption coefficient
V = volume of powder exposed to x-ray beam

A full derivation of this equation can be found in most advanced texts on x-ray diffraction. The first set of terms contains physical constants and machine-dependent terms and will be constant for the same machine operating under a given set of conditions, i.e. accelerating voltage and filament current. The second two sets of terms depend upon *hkl*. All of these terms in brackets can be combined into one term, K_{hkl}, which will be constant for any given diffraction peak under fixed operating conditions. Then one can write a simple expression for the intensity of a diffracted beam which depends only on K_{hkl}, on the volume of powder in the beam, V, and on the linear absorption coefficient of the powder, μ. This simplified expression is given below.

$$I_{hkl} = K_{hkl} \cdot \frac{V}{\mu} \tag{2}$$

To convert the above equation, which is for a single phase powder, to an equation for a multiphase mixture, V is replaced by V_i, the volume fraction of phase i in the mixture, and μ is replaced by μ_m, the linear absorption coefficient of the mixture.

$$I_i = K_i \cdot \frac{V_i}{\mu_m} \tag{3}$$

The *hkl* subscripts have been dropped from I_{hkl} and K_{hkl}, and the subscript i has been added. For I_i, this subscript identifies the intensity of a selected peak of phase i in the mixture. Similarly, K_i is a constant for a selected peak of phase i. It is desirable to convert V_i in equation 3 to X_i, the weight fraction of component i in the mixture. To do this, V_i is replaced by X_i/ρ_i, where ρ_i is the density of phase i. Thus,

$$I_i = K_i \cdot \frac{X_i}{\rho_i \mu_m} \tag{4}$$

3.2 Working Equation

By taking the ratio I_i/I_c, where I_c is the intensity for a given peak of a reference material which has been added to the mixture in a known quantity, X_c, one obtains the working equation for the quantitative analysis of mixtures.

$$\frac{I_i}{I_c} = \frac{K_i}{K_c} \cdot \frac{X_i}{X_c} \cdot \frac{\rho_c}{\rho_i} \cdot \frac{\mu_m}{\mu_m} = k_i \cdot \frac{X_i}{X_c} \tag{5}$$

The subscript c is used to denote corundum(α-Al_2O_3) which has been established by the Joint Committee on Powder Diffraction Standards as a standard reference material because of its purity, ready availability, and high stability. k_i is known as the reference intensity ratio for phase i in the mixture.

The selection of peaks for k_i determination is arbitrary. Typically, the most intense diffraction peak of each phase is chosen, but in multicomponent systems it is often necessary to choose not the most intense reflection, but the most intense resolved

reflections. If a peak is selected for k_i determination which is not the most intense peak for that phase, the measured intensity can be scaled to the value of the most intense peak by comparison with a pure sample of the phase, or the selected peak can be used directly. The only requirement is that consistency be maintained throughout. Values of k_i are tabulated for the strongest reflections of many phases in the JCPDS card file for $X_i = X_c = 0.5$. However, it is best to calculate the reference intensity ratios obtained for each material under the same instrumental conditions. This calculation is accomplished using equation 6, to calculate each k_i from data for a single multicomponent mixture of known composition.

$$k_i = \frac{I_i}{I_c} \cdot \frac{X_c}{X_i} \tag{6}$$

Once each of the k_i's has been determined, one can calculate the weight fraction of each phase in mixtures of unknown composition from the equation

$$X_i = \frac{I_i}{I_c} \cdot \frac{X_c}{k_i} \tag{7}$$

The above equation allows each X_i to be determined independently from the others, allowing in theory for the calculation of the weight fraction of unknown or even amorphous phases in a mixture by summing all of the known X_i's. The extent to which this determination can be accomplished depends on the error in measuring the individual X_i's.

3.3 Detection Limit and Sources of Error

The detection limit for component i in a mixture, X_i(d.l.), is defined as the minimum concentration required to produce an observable signal above the background signal. The background intensity, I_b, is typically taken as $3\sqrt{N_b}/t$, where N_b is the number of background counts accumulated over t seconds. Substituting I_b for I_i in equation (7) gives,

$$X_i(\text{d.l.}) = \frac{X_c}{I_c} \cdot \frac{I_b}{k_i} = \frac{X_c}{I_c} \cdot \frac{3\sqrt{N_b}}{k_i t} \tag{8}$$

One of the main sources of error in quantitative analysis by x-ray powder diffraction is variation in sample preparation. Great care must be taken to prepare all samples in as similar a manner as possible, and to operate the diffractometer under the same operating conditions. Preferred orientation of the particles exposed to the x-ray beam can occur, particularly if the crystallites are needle or plate-like in habit. The basic intensity equation for x-ray diffraction was derived for a random distribution of crystalline particles and is inaccurate if any preferred orientation exists. Errors due to preferred orientation can be reduced by adding the intensities of several peaks for one phase. This method of adding intensities also improves the counting statistics by increasing the total measured intensity for each phase.

3.4 Peak Selection for Quantitative Analysis and Phase Identification

Table 1 is a compilation of d-spacing, two-theta, and intensity values for all of the peaks of the barium titanate phases which might form during a solid state reaction. These values were taken from the JCPDS card file and sorted by increasing two-theta values. Each peak is identified by its composition and if known, its *hkl* indices. Phases for which the JCPDS patterns were questionable or of low quality are $Ba_2Ti_9O_{20}$ and $BaTi_2O_5$. Also included in Table 1 is the pattern for α-Al_2O_3(corundum), which was used as a reference material. Table 1 was scanned for isolated peaks of each phase for purposes of quantitative analysis and phase identification. The selected peaks are shown in Table 2, with the peaks being used for quantitative analysis denoted by QA.

The majority of peaks in Table 1 are not useful for quantitative analysis because of peak overlap. In the previous work by Templeton and Pask[4], peaks were selected which are shown in Table 1 to overlap with other peaks and are therefore not suitable for quantitative analysis. They used the 402,431 peak of "$BaTi_3O_7$" ($Ba_4Ti_{13}O_{30}$) which coincides with a peak of $BaTi_4O_9$, and the 121 peak of $BaTi_4O_9$ which overlaps a $Ba_2Ti_9O_{20}$ peak. The peaks which they selected can not be fully resolved because of this overlap and also because of the close proximity of the selected peaks themselves (31.4° and 31.3°), and they did not measure integrated intensity--they used the maximum peak height which in itself increases the error in their measurements.

The peaks selected for quantitative analysis in the present study were not always those of maximum intensity, but were sufficiently separated from neighboring peaks to be useful. The criterion that each peak be separated from neighboring peaks by at least 0.3° was used to select peaks for phase identification. For purposes of quantitative analysis the nearest neighbor peak distance was required to be 0.5° or greater. After it was determined that certain phases were not present in the mixtures, peaks of those phases were eliminated from the possibilities considered in Table 1 making possible the selection of peaks such as the 110 peak of Al_2O_3 which is only 0.1° degrees from the neighboring $BaTi_2O_5$ peak.

It is interesting to note that many of the peaks listed in Table 1 have the same d-spacing. For example, the 110 peak of TiO_2 and the 411 peak of $Ba_4Ti_{13}O_{30}$ coincide exactly. There are numerous other cases of coincidence in Table 1. Some of these coincident values could be in error because the JCPDS patterns of little studied phases are unreliable, but much of the overlap is caused by the close structural similarities of the various barium titanate phases[30].

4 Experimental Procedures

4.1 Methods of Characterization

The BET method for determining the specific surface areas of the different starting materials was used. The equipment used was a QuantaChrome QuantaSorb Surface Area Analyzer Model S-7.

Scanning electron microscopy (SEM) was performed on an ISI Model DS-130 high resolution microscope to determine the particle size, shape, and morphology of the starting materials, mixed powders, and reaction products.

A Siemens Diffractometer Model D500 was used for x-ray diffraction analysis of starting materials and reaction products. The starting materials were scanned from 20° to 70° at 0.1° intervals with a dwell time of 1 second to locate the various peaks. All of the reaction mixtures were scanned from 10° to 100° with a step-scan of 0.4°/step and a dwell time of 8 seconds. Duplicate runs of selected peaks were scanned over a 1° interval on each side of the peak with the same step-scan and dwell time. Data were stored on disk as a list of two-theta values and number of counts. These data were later analyzed using the Siemens Diffrac-11 software and computer programs written for the IBM-PC in Borland Turbo Pascal. Computer programs written for the IBM-PC were used to calculate a linear background line across each of the peaks selected for quantitative analysis and to calculate the integrated intensities of these peaks. The methods used for quantitative analysis were described in an earlier section.

4.2 Raw Materials

Both the TiO_2 (rutile) and $BaTiO_3$ powders were Puratronic grade purchased from Johnson Mathey Chemicals, Limited. Table 3 lists the batch numbers, impurities, and particle size data for each material. Indexed XRD patterns for each of the pure materials are shown in Figure 4. The pattern for rutile (Figure 4b) shows no trace of the anatase phase. SEM pictures of the two materials are shown in Figure 5. The TiO_2

powder consisted of agglomerates between 0.3 and 0.8 mm in diameter. These agglomerates were composed of irregularly shaped particles which ranged in size between 20 and 80 μm. The $BaTiO_3$ powder consisted of 8 - 40 μm particles.

The α-Al_2O_3 used as an internal standard for quantitative analysis was reagent grade from J.T. Baker Chemical Co. The powder was sieved through a #325 mesh screen to obtain a particle size below 45 μm. The impurities and batch number for this material are given in Table 3.

4.3 Sample Preparation

A Mixture of $BaTiO_3$ and TiO_2 ceramics was weighed on a Mettler H20C balance to one tenth of a milligram. The batch consisted of 16.9694g $BaTiO_3$ and 20.3492g TiO_2 corresponding to an overall stoichiometry of $Ba_2Ti_9O_{20}$. The powder mixture was milled in a plastic jar with ZrO_2 balls for 30 minutes in a high-speed planetary ball mill. Two gram pellets of the powder mixture were pressed to 50% theoretical density using a half inch die lubricated with zinc stearate.

The pellets were fired in air at 1050°C in a vertical tube furnace for various times from 24 minutes to 6 days, and removed from the furnace and allowed to air-cool. The pellets were then broken apart and one piece was saved for use in the SEM. The remainder was mixed with α-Al_2O_3 ($\approx$ 30 weight percent) and milled in the planetary ball mill using ZrO_2 balls in a plastic jar for 15 minutes. The exact weight proportions and sample identification codes for each sample are given in Table 4. The mixed fine powder was pressed into a lucite sample holder for use in XRD experiments. The dimensions in mm of the recessed area in the lucite sample block were 25 $\times$ 25 $\times$ 1.6.

For examination in the SEM, powder samples of the raw materials were held to Al sample mounts with double stick tape and were gold coated in a Polaron sputtering apparatus. Fracture surfaces of fired pellets were examined after the pieces were mounted with epoxy onto a sample mount and gold coated.

5 Experimental Results and Data Reduction

5.1 SEM Observations

Figure 6 is an SEM micrograph (126×) of the unfired mixed powders mounted on double-stick tape after grinding in the planetary ball mill. The large TiO_2 agglomerates have been broken up so that the largest TiO_2 particles are ≈ 80 μm across. Higher magnification photographs (500×) of the TiO_2 particles revealed smooth surfaces.

As the reaction proceeded, sub-micron particles were formed out of the original TiO_2 particles. This process is shown in Figure 7. The micrograph of Figure 7 (2400×) was prepared from sample S06D after mixing with Al_2O_3 and grinding. The particle shown is roughly 50 μm across. Figure 8 is a micrograph (2240×) of a fracture surface from sample S08H which also shows the overall transformation of the large particle starting materials into sub-micron product phase particles.

5.2 XRD Data Reduction

X-ray patterns for each of the samples are shown in Figures 9. Figure 9a shows the data in the two-theta range 10-40°, Figure 9b shows the data in the range 40-70°, and Figure 9c shows the data in the range 70-100°. The d-spacings and integrated intensities for the peaks in each pattern are given in Table 5(a-h). The calculation of d-spacings and integrated intensities were done with the Siemens Diffrac-11 IDR software program. This program was found to give consistent values for the d-spacings, which were taken at the point where the second derivative of the curve fit through the raw data points was a minimum[33], but the integrated intensity values were suspected of being in error. It was found that the program did not correctly subtract out the background. The intensities calculated by the program appear to be fairly self-consistent, but for purposes of quantitative analysis it was necessary to calculate the integrated intensities of selected peaks by hand.

Another problem with using the IDR program was in adjusting the "sensitivity factor" which controls how the program determines the presence of peaks. In several instances low intensity peaks are not reported by the IDR program. When this occurred for peaks which were selected for quantitative analysis and phase identification, careful inspections of the peaks were made graphically. This process will be described in section 5.3 below. If a peak was found to be present, a line was added to the IDR data shown in Table 5.

The process of analyzing the x-ray data given in Table 5 for phase identification did not follow easily from the data in Table 1. In cases where a peak could be assigned to more than one phase, additional peaks for each of the phases were sought to confirm the presence of that phase. By eliminating phases which were not present (or below the detection limit), the number of phases in Table 1 could be reduced significantly so that each peak could be assigned unambiguously. However, where overlap occurred with two peaks from phases which were both known to be present, the peak was assigned to both phases. The resulting peak assignments are shown in Table 5 with the d-spacing and intensity data.

The raw data for quantitative analysis were analyzed in the following way. Data for selected peaks were extracted from the original data files. A linear background line was determined for each peak by averaging three background points on each side of the peak and fitting a straight line between them. The integrated intensity was taken as the area under the raw data curve above the calculated background line. An example of this procedure is shown in Figure 10a for the 101 peak of TiO_2 and Figure 10b for the 022,040 peak of $Ba_4Ti_{13}O_{30}$. The resulting intensity values for each peak were averaged for the duplicate runs and the averaged values divided by the dwell time (8 seconds) to convert counts to counts per second (cps). The intensities for each of the phases followed by quantitative analysis were taken as the sum of the intensities of the selected peaks. These values are listed in Table 6a.

5.3 Phase Identification

Because the data of Table 5 did not always unambiguously establish the presence of the possible intermediate phases, careful examination was made of the peaks selected for this purpose as given in Table 2. The intensity of the 031 peak of $BaTi_4O_9$ as a function of time is shown in Figure 11. The intensity of the (022,040) peak of $Ba_4Ti_{13}O_{30}$ is shown in Figure 12, and both the 021 peak of $BaTi_4O_9$ and the (102, 131) peak of $Ba_4Ti_{13}O_{30}$ are shown in Figure 13. Both $BaTi_4O_9$ and $Ba_4Ti_{13}O_{30}$ were detected after only 24 minutes.

The presence of $BaTi_4O_9$ after 24 minutes is clearly evident from inspection of Figure 11 and 13, but the presence of $Ba_4Ti_{13}O_{30}$ at this early time is not as obvious. To confirm the presence of $Ba_4Ti_{13}O_{30}$ the intensity data of the 022,040 peak was checked for statistical significance above the background level. The average background intensity on both sides of the peak is ~17 cps. Peak intensities were considered to be significant if they were three standard deviations above the background intensity. Three standard deviations corresponds to ~12 cps above background. From the data of Table 6, $Ba_4Ti_{13}O_{30}$ is shown to be present with an intensity of 18 cps above background. Figure 10b shows the calculated background line and intensity data for the this peak after 24 minutes at temperature.

Although the overall sample stoichiometry was in the correct ratio for the formation of $Ba_2Ti_9O_{20}$, this phase was not detected until after 8 hours at temperature. In Figure 14a, the $Ba_2Ti_9O_{20}$ peak can be resolved for sample S08H, but the $Ba_2Ti_9O_{20}$ peak which should be present in Figure 14b is not clearly resolved for any of the samples. The selected $Ba_2Ti_9O_{20}$ peak should be found at 60.806°, but inspection of the Figure shows a peak between 60.68 and 60.72°. It is possible that the peak at 60.68° is the selected $Ba_2Ti_9O_{20}$ peak and that the data in the JCPDS card file is in error. However, it is also possible that the peak at 60.68° is an unidentified peak from one of the other phases which were present. For sample S06D in Figure 14a, it appears as though a peak might be present at 60.80°, but due to the close proximity of the peak at 60.68° it is not possible to establish the presence of the $Ba_2Ti_9O_{20}$ peak.

Careful examination was made of the two-theta range about the selected $Ba_6Ti_{17}O_{40}$ peak. Although $Ba_6Ti_{17}O_{40}$ is reported to be a thermodynamically stable phase of the BaO - TiO_2 system, there was no indication of its presence. Similarly, $BaTi_5O_{11}$, which O'Bryan and Thomson report to form when $BaCO_3$ and TiO_2 are heated together at 1100°C, was not observed and no evidence for the presence of the metastable phases $BaTi_6O_{13}$ or $BaTi_2O_5$ was found.

A summary of the phases which were positively identified for the various times at temperature is given in Table 7. Phases which were not found are marked with an X, and phases which were found are denoted ***.

5.4 Quantitative Analysis

Reference intensity ratios for $BaTiO_3$ and TiO_2 were calculated from equation 6 using the intensity values and weight fractions from sample Sraw. Using these reference intensity ratios, the weight fractions of TiO_2 and $BaTiO_3$ in each sample were calculated using equation 7. These results are plotted in Figure 15 where the weight fractions have been divided by $(1-X_c)$ to make them relative to the reaction mixture without the added Al_2O_3. Also shown in Figure 15 is the weight fraction of intermediate phases calculated as one minus the weight fractions of $BaTiO_3$ and TiO_2.

The amount of $BaTiO_3$ and TiO_2 after 6 days was 21.5 w/o and 28.9 w/o, respectively. The composition of the starting material was 45.5 w/o $BaTiO_3$ and 54.5 w/o TiO_2. This large amount of unreacted powder can be attributed to the size of the original TiO_2 particles. These were intentionally chosen to be large so that by slowing the reaction rate the various intermediate phases might be observed more easily. It is also possible that the reaction mixture was heterogeneous and that local equilibrium was approached in isolated regions causing the rate of the reaction to decrease.

It was not possible to calculate reference intensity ratios for $BaTi_4O_9$, $Ba_4Ti_{13}O_{30}$, and $Ba_2Ti_9O_{20}$ directly because pure samples of these phases were not available. An attempt was made to determine k_i values for $BaTi_4O_9$ and $Ba_4Ti_{13}O_{30}$ from the data of samples S24m, S01H, and S02H for which these were the only intermediate phases

present. These calculated k_i values could then be used to determine the amounts of these phases in each of the samples. In the samples which were heated for 8 hours or more, the amount of $Ba_2Ti_9O_{20}$ would be determined by $1 - \Sigma X_i$, where X_i includes all of the other phases which were present.

However, consistent values of k_i for $BaTi_4O_9$ and $Ba_4Ti_{13}O_{30}$ could not determined from the three samples due to the scatter in the data. Instead, a plot of normalized intensities for these two phases is shown in Figure 16. The intensities were normalized by use of the multiplier $(X_c/I_c)/(1-X_c)$. These values differ from the true weight fractions of these phases in the reaction mixture only by the reference intensity ratio. Normalized intensity values were not determined for $Ba_2Ti_9O_{20}$ because overlapping of peaks made it difficult to get good intensity data for this phase.

An approximate value of the detection limit for each of the observed phases was determined from equation 8 by use of estimated relative intensity ratios. If a value of ~1-2 is taken for the relative intensity ratio and an average background intensity of ~ 130 counts/8s is used, a value of 2-4 w/o is calculated. At higher angles the background intensity is reduced to ~60 counts/8s, and for similar values of k_i the detection limit is calculated as 1.5 - 3 w/o. The detection limits for $BaTi_4O_9$ and for $Ba_4Ti_{13}O_{30}$ were observed to be less than 3.5 w/o in sample S24M, where 3.5 w/o is the total amount of intermediate phases observed in the sample. The actual detection limits for $BaTi_4O_9$ and $Ba_4Ti_{13}O_{30}$ are probably closer to 2 w/o. This value of the detection limit would be decreased if higher intensity peaks could be resolved without overlap with neighboring peaks.

6 Discussion

In this study the technique of quantitative analysis by x-ray diffraction has been applied to the study of intermediate phase formation between $BaTiO_3$ and TiO_2. It seemed likely that some of the phases of compositions between $BaTiO_3$ and TiO_2 are present during reaction between $BaCO_3$ and TiO_2, but have gone undetected a) because their quantities were low compared to those of the reactants and of $BaTiO_3$ and Ba_2TiO_4 and b) because overlap of the diffraction peaks of the various phases makes analysis difficult.

To increase the effective volume fraction of intermediate phases, the reaction of $BaTiO_3$ with large particles of TiO_2 was studied. The problem of peak overlap was greatly simplified by elimination of $BaCO_3$ and Ba_2TiO_4 from the system. A careful selection of reference peaks was made to establish the presence of the known barium titanate phases. Using computer assisted evaluations it then was possible to establish which phases were present and to determine the total amount of intermediate phases with greater accuracy than possible in previous studies.

Three phases were observed in the reaction between $BaTiO_3$ and TiO_2: $BaTi_4O_9$, $Ba_4Ti_{13}O_{30}$, and $Ba_2Ti_9O_{20}$. $BaTi_4O_9$ and $Ba_4Ti_{13}O_{30}$ formed readily and were observed after only 24 minutes at 1050°C. Values of normalized intensity, which scale with the weight fraction of the phases, are plotted in Figure 16 as a function of time. $BaTi_4O_9$ initially grows rapidly in amount, but stays relatively constant after 24 hours. $Ba_4Ti_{13}O_{30}$ also forms rapidly at the start of the reaction, but its amount continues to increase at a steady rate throughout the time interval examined in this study(144 hours). The data of Figure 16 is replotted in Figure 17 as normalized intensity against the square root of time. The essentially linear plot for $Ba_4Ti_{13}O_{30}$ indicates that the formation of this phase could be diffusion controlled.

$Ba_2Ti_9O_{20}$ was not observed until after 8 hours into the reaction. This delay indicates that a nucleation barrier might exist for the formation of this phase. After 8 hours, the intensity of the selected $Ba_2Ti_9O_{20}$ peaks is seen to increase with time (Figure 14) indicating normal growth.

$Ba_6Ti_{17}O_{40}$ is the only equilibrium barium titanate phase of composition between those of the two reactants which was not observed during the course of the reaction. It is possible that $Ba_6Ti_{17}O_{40}$ did form, but in an amount below the detection limit (~3 w/o). More probably, however, $Ba_6Ti_{17}O_{40}$ was prevented from forming by a nucleation barrier.

$BaTi_5O_{11}$, which was found by O'Bryan and Thomson in a mixture of the same stoichiometry as the mixture used in this study and at a similar reaction temperature (1100°C), was not observed during the course of reaction. Perhaps $BaTi_5O_{11}$ is stable at 1100°C, but not at 1050°C or perhaps it is stabilized by CO_2 or by impurities present in O'Bryan and Thomson's mixture but not present in the mixture used in this study. The detection techniques used in the present study should have identified $BaTi_5O_{11}$ if it were present in the quantities found by O'Bryan and Thomson. $BaTi_6O_{13}$ and $BaTi_2O_5$ were also not observed, but since these phases form only from samples which have been melted and are thought not to be equilibrium phases at 1050°C, their absence was expected.

Templeton and Pask[4] studied the formation of $BaTiO_3$ from equimolar mixtures of $BaCO_3$ and TiO_2, heated at different temperatures and in different atmospheres. Their data for an equimolar mixture of $BaCO_3$ and TiO_2, heated at 1050°C in air, are shown in Table 8 for comparison with the data of Table 7. At the time of their work, not all of the phases in the BaO-TiO_2 system were known, but they were able to identify Ba_2TiO_4, $BaTiO_3$, $Ba_4Ti_{13}O_{30}$, and $BaTi_4O_9$ after only 15 minutes at 1050°C. In their Table, they report the mole fractions of these phases, but the peaks which they selected for quantitative analysis have been shown to overlap with peaks from other phases.

Templeton and Pask concluded that $BaTiO_3$ forms initially at the $BaCO_3$ - TiO_2 interface. After this initial step, Ba_2TiO_4 is reported to form between the $BaTiO_3$ layer and $BaCO_3$, and $Ba_4Ti_{13}O_{30}$ and $BaTi_4O_9$ to form between the $BaTiO_3$ layer and TiO_2. Assuming this model, the reaction which proceeds into the TiO_2 ceramic can be viewed

as a reaction between $BaTiO_3$ and TiO_2, and the formation of $Ba_4Ti_{13}O_{30}$ and $BaTi_4O_9$ is expected from examination of the phase diagram (Figure 2) if local thermodynamic equilibrium is approached and if nucleation occurs.

The results of the present study, as well as the results of Templeton and Pask, show that $Ba_4Ti_{13}O_{30}$ and $BaTi_4O_9$ form readily with no apparent nucleation barrier. With this fact in mind, it does not seem likely that $BaTiO_3$ is the first phase formed at the TiO_2 interface. It is more likely that $BaTi_4O_9$, $Ba_4Ti_{13}O_{30}$, and $BaTiO_3$ all form as soon as a reaction begins in order of their variation in BaO/TiO_2 content. This new model is consistent with the experimental observation that all of the phases described above are present in the reaction mixture of $BaCO_3$ and TiO_2 after only 15 minutes at 1050°C (Table 8). If diffusion through $Ba_4Ti_{13}O_{30}$ and $BaTi_4O_9$ is rapid, the relative thickness of these phases will be small, and hence the volume fractions will be small compared with those of $BaTiO_3$ and Ba_2TiO_4.

In mixtures of $BaCO_3$ and TiO_2 heated at temperatures below 800°C, Cournil, Soustelle, and Thomas[6a] report that $BaTiO_3$ was the only phase formed. For the same reaction, Templeton and Pask[4] report a small amount (1 mole %) of $Ba_4Ti_{13}O_{30}$ after only one hour at 900°C and after 36 hours at 750°C, and they report a small amount of $BaTi_4O_9$ (1 mole %) after 22 hours at 750°C. Therefore, it is probable that these phases were also present in the samples of Cournil, et. al., but in amounts which were too small to detect.

In a second paper, Cournil, et. al.[6b] develop a detailed model in which TiO_2 is converted directly to $BaTiO_3$ during reaction with $BaCO_3$ by a series of reaction steps at various assumed interfaces. The authors then try to explain the effect of different gaseous atmospheres on the reaction rates in terms of their model. Their mechanistic approach should be considered with caution, however, because of their assumption that higher titanate phases do not form at the TiO_2 interface.

In a study of the formation of $BaTiO_3$, Beauger, Mutin, and Niepce[5b] examined various interface reactions by scanning electron microscopy and electron probe microanalysis. Their samples consisted of sintered pellets of $BaCO_3$, Ba_2TiO_4, $BaTiO_3$,

and TiO_2 which were stacked together in different ways and heated at various temperatures. In their study of the $BaTiO_3$ - TiO_2 interface, they report the formation of a phase richer in titanium than $BaTiO_3$ in the TiO_2 ceramic, but the composition of the phase was not determined. They attribute the formation of this phase to the "excessive thickness" of the $BaTiO_3$ layer because they did not observe this phase when they calcined intimately mixed micrometric powders.

The results of the present study show that $Ba_4Ti_{13}O_{30}$ and $BaTi_4O_9$ form readily by reaction of $BaTiO_3$ and TiO_2. Therefore, the unknown "phase" which was observed in the TiO_2 was most likely two phases: $Ba_4Ti_{13}O_{30}$, and $BaTi_4O_9$. The statement about the excessive thickness of the $BaTiO_3$ layer being responsible for the formation of these phases deserves comment. The formation of a reaction product at an interface between two reactants depends only on the activity of each species at the interface and on the kinetic barrier which might keep a phase from forming. The thickness of the two reactants is unlikely to determine which phases are formed, but might determine which phases are detected if the reactants are much thicker than the product phases. The fact that these phases were not observed in the reaction of fine powders can be explained by the rapid rate of $BaTiO_3$ formation from fine powders.

In the work by Amin, Spears, and Kulwicki[22], the reaction of $BaCO_3$ with anatase and with rutile was followed by several techniques including x-ray diffraction. Their report of the presence of $Ba_4Ti_{13}O_{30}$ is based on the identification of a diffraction peak at 28.4° as the "principal peak" of this phase. The position of this peak from the data of Table 1 is 28.267°. The 022,040 peak of $BaTi_4O_9$ lies at 28.358°. Therefore, the peak found by Amin, et. al. at 28.5° might alternatively be attributed to this phase. Furthermore, their measurements, which are reported only for the two-theta range 22.7 - 35.5°, show the presence of a peak at ~26.0° after 1800s and 3600s at 910°C. If $Ba_4Ti_{13}O_{30}$ and $BaTi_4O_9$ are considered to be the only intermediate phases formed, this peak could be assigned as the 302 peak of $Ba_4Ti_{13}O_{30}$ (26.178° in Table 1). A peak at ~23.0° is observed in their data for the sample heated 1800s. It is possible that this is the 031 peak of $BaTi_4O_9$ (at 23.197° in Table 1).

7 Conclusion

Careful analysis of the $BaTiO_3$ - TiO_2 reaction by x-ray diffraction has shown that $Ba_4Ti_{13}O_{30}$ and $BaTi_4O_9$ form readily without a significant nucleation barrier. The work of several other authors[4,5,6,22] was reexamined in light of these observations. The assumption that $BaTiO_3$ is the first phase formed at the TiO_2 interface during reaction of $BaCO_3$ and TiO_2 has been questioned. An alternate model is suggested in which each of the barium titanate phases which form without a significant nucleation barrier are formed in order of highest TiO_2 content by diffusion into TiO_2. Thus, $BaTi_4O_9$ is the first phase formed, followed by the formation of $Ba_4Ti_{13}O_{30}$, and $BaTiO_3$. The reported absence of $Ba_4Ti_{13}O_{30}$ and $BaTi_4O_9$ in many studies can be attributed to their being present in low volume fractions because diffusion through their layers is rapid.

References

1. H.M. O'Bryan, Jr., J. Thomson, Jr. and J.K. Plourde, *J. Amer. Cer. Soc.*, **57**(10) 450-453 (1974)
2. T. Kubo and K. Shinriki,
   a. *J. Chem. Soc. Japan, Ind. Chem. Sect.* **54** 268-270 (1951)
   b. *J. Chem. Soc. Japan, Ind. Chem. Sect.* **54** 358-361 (1951)
   c. *J. Chem. Soc. Japan, Ind. Chem. Sect.* **55** 49-51 (1952)
   d. *J. Chem. Soc. Japan, Ind. Chem. Sect.* **55** 137-140 (1952)
   e. *J. Chem. Soc. Japan, Ind. Chem. Sect.* **56** 149-151 (1953)
   f. *J. Chem. Soc. Japan, Ind. Chem. Sect.* **55** 335-337 (1953
3. T. Kubo, M. Kato, and T. Fujitas,
   a. *Kogyo Kagaku Zasshi* **70(6)** 847-53 (1967)
   b. *Kogyo Kagaku Zasshi* **71(1)** 114-18 (1968)
4. L. K. Templeton and J. A. Pask, *J. Amer. Cer. Soc.* **42**(5) 212-216 (1959)
5. A. Beauger, J. C. Mutin, and J. C. Niepce,
   a. *J. Mater. Sci.* **18** 3041-3046 (1983)
   b. *J. Mater. Sci.* **18** 3543-3550 (1983)
6. M. Cournil, M. Soustelle, and G. Thomas,
   a. *Oxid. Met.* **13**(1) 77-88 (1979)
   b. *Oxid. Met.* **13**(1) 89-104 (1979)
7. H. M. O'Bryan and M. F. Yan, *J. Amer. Cer. Soc.* **65**(12) 615-618 (1982)
8. T. Nakayama and T. Sasaki, *Bull. Chem. Soc. Jpn.* **36** 569-574 (1963)
9. A. N. Toropov, A. I. Borisenko, D. V. Semilatova, L. I. Yankovskaya, *Zh. Prik. Khim.* (Leningrad) **41**(11) 2368-2374 (1968)
10. A. Mangel and J. Doskocil, *Silikaty* **13**(1) 12-28 (1969)
11. J. Murray, *Amer. Cer. Soc. Bull.* **37**(11) 476-479 (1958)
12. J.C. Mutin and J.C. Niepce, *J. Mater. Sci. Lett.*, **3** 591-592 (1984)
13. O. Eibl, P. Pongratz, P. Skalicky, and H. Schmelz, *J. Amer. Cer. Soc.*, **70**(8) C195-C197 (1987)

14. Y. Suyama and A. Kato,

    a. *Ceramurgia International* **1(1)** 5-9 (1975)
    b. *Ceramurgia International* **1(3)** 123-126 (1975)
    c. *Bull. Chem. Soc. Jpn.* **50(6)** 1361-1366 (1977)

15. H. M. O'Bryan and J. Thomson, *J. Amer. Cer. Soc. Disc. and Notes* **58**(9-10) 454 (1975)

16. E. Tillmanns, *Acta Cryst.*, **B25**(8) 1444-1452 (1969)

17. E. Tillmanns, *Cryst. Struct. Comm.* **1**(1) 1-4 (1972)

18. H.M. O.Bryan, Jr. and J. Thomson, Jr., *J. Amer. Cer. Soc.* **57**(12) 522-526 (1974)

19. G.H. Jonker and W. Kwestroo, *J. Amer. Cer. Soc.*, **41**(10) 1958

20. H. Schmalzried, "Solid State Reactions", Academic Press, New York (1974)

21. M. Gavoglio and D. Beruto, *Ceramics International* **10(4)** 132-134 (1984)

22. A. Amin, M. A. Spears, B. M. Kulwicki, *J. Amer. Cer. Soc.* **66**(10) 733-738 (1983)

23. M. Cournil and G. Thomas, *J. Thermal Anal.*, **17** 435-455 (1979)

24. W. Hofmeister, E. Tillmanns and W.H. Baur, *Acta Cryst.* **C40** 1510-1512 (1984)

25. T. Negas, R. S. Roth, H. S. Parker, and D. Minor, *J. Sol. State. Chem.* **9** 297-307 (1974)

26. E. Tillmanns, *Inor. Nucl. Chem. Lett.* **7** 1169-1171 (1971)

27. D. E. Rase and R. Roy, *J. Amer. Cer. Soc.* **38**(3) 102-113 (1955)

28. H. M. O'Bryan and J. Thomson, *J. Amer. Cer. Soc.* **66**(1) 66-68 (1983)

29. H. J. Hageman and H. M. O'Bryan, *J. Amer. Cer. Soc.* **70**(4) 274-278 (1987)

30. E. Tillmanns and W. Hofmeister, *J. Sol. St. Chem.* **58** 14-28 (1985)

31. F. H. Chung,

    a. *J. Appl. Cryst.* **7** 519-525 (1974)
    b. *J. Appl. Cryst.* **7** 526-531 (1974)
    c. *J. Appl. Cryst.* **8** 17-19 (1975)

32. H. P. Klug and L. E. Alexander, "X-ray Diffraction Procedures", John Wiley, New York (1959)

33. Siemens Diffrac-11 Users Manual

TABLE 1 : Xray Diffraction Data For Barium Titanate Phases

2θ(deg)	d(Å)	I/I_{max}	hkl	Phase
11.406	7.7519	20	120	$Ba_6Ti_{17}O_{40}$
13.981	6.3291	11	220	$Ba_6Ti_{17}O_{40}$
15.316	5.7803	20	011	$BaTi_4O_9$
16.296	5.4348	15	211, 220	$Ba_4Ti_{13}O_{30}$
17.189	5.1546	10	120	$BaTi_5O_{11}$
18.619	4.7619	15	021	$BaTi_4O_9$
18.976	4.6729	15	131	$Ba_6Ti_{17}O_{40}$
19.066	4.6512	25	102, 131	$Ba_4Ti_{13}O_{30}$
19.334	4.5872	30	200	$BaTi_2O_5$
20.769	4.2735	60	022, 040	$Ba_4Ti_{13}O_{30}$
21.307	4.1667	50	140	$Ba_6Ti_{17}O_{40}$
21.577	4.1152	10	-104, 004	$BaTi_2O_5$
22.026	4.0323	40	231	$Ba_4Ti_{13}O_{30}$
22.026	4.0323	12	001	$BaTiO_3$
22.296	3.9841	25	100	$BaTiO_3$
22.476	3.9526	25	031	$BaTi_5O_{11}$
23.197	3.8314	40	031	$BaTi_4O_9$
23.467	3.7879	50	200	$BaTi_5O_{11}$
23.828	3.7313	35	-322, 331	$Ba_6Ti_{17}O_{40}$
23.828	3.7313	35	002	$BaTi_5O_{11}$
23.918	3.7175	15		$Ba_2Ti_9O_{20}$
24.640	3.6101	9	-511	$Ba_6Ti_{17}O_{40}$
25.182	3.5336	35		$Ba_2Ti_9O_{20}$
25.273	3.5211	12	400	$Ba_4Ti_{13}O_{30}$
25.363	3.5088	40	040	$BaTi_5O_{11}$
25.545	3.4843	15	-204, 104	$BaTi_2O_5$
25.907	3.4364	40	11-2	$BaTi_5O_{11}$
26.178	3.4014	30	302	$Ba_4Ti_{13}O_{30}$
26.269	3.3898	60		$Ba_2Ti_9O_{20}$
25.545	3.4843	75	210	Al_2O_3
26.632	3.3445	40	220	$BaTi_5O_{11}$
27.085	3.2895	45	022	$BaTi_5O_{11}$
27.085	3.2895	55		$Ba_2Ti_9O_{20}$
27.267	3.2680	30	431, 511	$Ba_6Ti_{17}O_{40}$
27.42	3.25	40	100	$BaTi_4O_9$
27.448	3.2468	60	411	$Ba_4Ti_{13}O_{30}$
27.448	3.2468	100	110	TiO_2
27.631	3.2258	30	051	$Ba_6Ti_{17}O_{40}$
27.903	3.1949	30	013	$Ba_6Ti_{17}O_{40}$
27.994	3.1847	50	-213	$Ba_6Ti_{17}O_{40}$
27.994	3.1847	100	140, 041	$BaTi_5O_{11}$
28.267	3.1546	60	402	$Ba_6Ti_{17}O_{40}$
28.267	3.1546	100	322, 113+	$Ba_4Ti_{13}O_{30}$
28.267	3.1546	10	-113	$BaTi_2O_5$
28.358	3.1447	80	002, 041	$BaTi_4O_9$
28.449	3.1348	100		$Ba_2Ti_9O_{20}$
28.631	3.1153	20	600	$Ba_6Ti_{17}O_{40}$
28.723	3.1056	10	-302	$BaTi_2O_5$
28.814	3.0960	85	-251, -531	$Ba_6Ti_{17}O_{40}$
29.179	3.0581	90	-611, 113+	$Ba_6Ti_{17}O_{40}$
29.179	3.0581	85		$Ba_2Ti_9O_{20}$
29.270	3.0488	30	300	$BaTi_2O_5$
29.726	3.0030	100	---	$BaTi_2O_5$
29.909	2.9851	60	-342	$Ba_6Ti_{17}O_{40}$
29.909	2.9851	100	130	$BaTi_4O_9$
30.000	2.9762	25		$Ba_2Ti_9O_{20}$
30.091	2.9674	100	121	$BaTi_4O_9$
30.274	2.9499	7	242	$Ba_6Ti_{17}O_{40}$
30.457	2.9326	30	213, 242	$Ba_4Ti_{13}O_{30}$
30.732	2.9070	100	221	$BaTi_5O_{11}$

TABLE 1 (cont.) : Xray Diffraction Data For Barium Titanate Phases

2θ(deg)	d(Å)	I/I_{max}	hkl	Phase
30.732	2.9070	15	113	$BaTi_2O_5$
30.732	2.9070	20		$Ba_2Ti_9O_{20}$
30.915	2.8902	50	20-2	$BaTi_5O_{11}$
31.190	2.8653	10	211	$BaTi_2O_5$
31.282	2.8571	85	402, 431	$Ba_4Ti_{13}O_{30}$
31.282	2.8571	5	???	$BaTi_4O_9$
31.373	2.8490	100	-133, 060	$Ba_6Ti_{17}O_{40}$
31.465	2.8409	40	13-2	$BaTi_5O_{11}$
31.465	2.8409	100	101	$BaTiO_3$
31.648	2.8249	100	110	$BaTiO_3$
31.832	2.8090	40	351	$Ba_6Ti_{17}O_{40}$
32.015	2.7933	60	133	$Ba_4Ti_{13}O_{30}$
32.015	2.7933	55		$Ba_2Ti_9O_{20}$
32.291	2.7701	30	-304	$BaTi_2O_5$
32.475	2.7548	8	342	$Ba_6Ti_{17}O_{40}$
32.659	2.7397	10	006	$BaTi_2O_5$
32.751	2.7322	9	-631	$Ba_6Ti_{17}O_{40}$
32.751	2.7322	30		$Ba_2Ti_9O_{20}$
32.935	2.7174	12	422, 440	$Ba_4Ti_{13}O_{30}$
33.488	2.6738	10	302	$BaTi_2O_5$
33.579	2.6667	25		$Ba_2Ti_9O_{20}$
33.672	2.6596	75	313, 342+	$Ba_4Ti_{13}O_{30}$
33.949	2.6385	20	522	$Ba_6Ti_{17}O_{40}$
33.949	2.6385	10	260	$Ba_4Ti_{13}O_{30}$
33.949	2.6385	50	032, 051	$BaTi_4O_9$
34.041	2.6316	9	-513	$Ba_6Ti_{17}O_{40}$
34.503	2.5974	20	451	$Ba_6Ti_{17}O_{40}$
35.151	2.5510	90	104	Al_2O_3
35.151	2.5510	9	720	$Ba_6Ti_{17}O_{40}$
35.706	2.5126	50	-301, 24-1	$BaTi_5O_{11}$
36.077	2.4876	50	101	TiO_2
36.448	2.4631	11	602, 062+	$Ba_6Ti_{17}O_{40}$
36.448	2.4631	10	004, 062	$Ba_4Ti_{13}O_{30}$
36.635	2.4510	25		$Ba_2Ti_9O_{20}$
36.728	2.4450	15	502, 531	$Ba_4Ti_{13}O_{30}$
37.007	2.4272	11	-731, -262	$Ba_6Ti_{17}O_{40}$
37.100	2.4213	20	102, 060	$BaTi_4O_9$
37.287	2.4096	20		$Ba_2Ti_9O_{20}$
37.752	2.3810	40	110	Al_2O_3
37.846	2.3753	10	-313	$BaTi_2O_5$
38.407	2.3419	8	262	$Ba_6Ti_{17}O_{40}$
38.501	2.3364	15	124, 153+	$Ba_4Ti_{13}O_{30}$
38.593	2.3310	15	542	$Ba_6Ti_{17}O_{40}$
38.593	2.3310	15	115, 311	$BaTi_2O_5$
38.874	2.3148	45	111	$BaTiO_3$
39.062	2.3041	10	122, 150	$BaTi_4O_9$
39.154	2.2989	20		$Ba_2Ti_9O_{20}$
39.154	2.2989	8	200	TiO_2
39.248	2.2936	50	400	$BaTi_2O_5$
39.436	2.2831	35	204, 271	$Ba_6Ti_{17}O_{40}$
39.998	2.2523	35	-462	$Ba_6Ti_{17}O_{40}$
40.186	2.2422	15	253, 271	$Ba_4Ti_{13}O_{30}$
40.186	2.2422	55		$Ba_2Ti_9O_{20}$
40.282	2.2371	20		$BaTi_2O_5$
40.376	2.2321	11	362, 253	$Ba_6Ti_{17}O_{40}$
41.222	2.1882	25	111	TiO_2
41.412	2.1786	80	304, 362	$Ba_4Ti_{13}O_{30}$
41.412	2.1786	50	232	$BaTi_5O_{11}$
41.695	2.1645	1	006	Al_2O_3
41.790	2.1598	20	132, 151	$BaTi_4O_9$

TABLE 1 (cont.) : Xray Diffraction Data For Barium Titanate Phases

2θ(deg)	d(Å)	I/I_{max}	hkl	Phase
41.979	2.1505	75		$Ba_2Ti_9O_{20}$
42.073	2.1459	25	-471	$Ba_6Ti_{17}O_{40}$
42.735	2.1142	65	462	$Ba_6Ti_{17}O_{40}$
42.735	2.1142	25	602, 324	$Ba_4Ti_{13}O_{30}$
42.830	2.1097	20	161	$BaTi_5O_{11}$
43.021	2.1008	55		$Ba_2Ti_9O_{20}$
43.209	2.0921	50	402	$BaTi_2O_5$
43.400	2.0833	100	113	Al_2O_3
43.400	2.0833	45	-604	$Ba_6Ti_{17}O_{40}$
43.495	2.0790	45	144	$Ba_6Ti_{17}O_{40}$
43.971	2.0576	20	-208, -117	$BaTi_2O_5$
44.065	2.0534	11	640	$Ba_4Ti_{13}O_{30}$
44.065	2.0534	10	210	TiO_2
44.160	2.0492	50	340	$BaTi_5O_{11}$
44.352	2.0408	8	404, -813+	$Ba_6Ti_{17}O_{40}$
44.542	2.0325	20		$Ba_2Ti_9O_{20}$
44.637	2.0284	30	242	$BaTi_5O_{11}$
44.828	2.0202	8	380, 453	$Ba_6Ti_{17}O_{40}$
44.828	2.0202	15	017	$BaTi_2O_5$
44.828	2.0202	12	002	$BaTiO_3$
44.924	2.0161	55	404, 462	$Ba_4Ti_{13}O_{30}$
45.019	2.0121	40		$BaTi_4O_9$
45.116	2.0080	15	-662	$Ba_6Ti_{17}O_{40}$
45.306	2.0000	11	533	$Ba_4Ti_{13}O_{30}$
45.402	1.9960	10	-217	$BaTi_2O_5$
45.402	1.9960	35	200	$BaTiO_3$
45.593	1.9881	15	562, 424	$Ba_6Ti_{17}O_{40}$
46.169	1.9646	2	202	Al_2O_3
46.169	1.9646	15	020	$BaTi_2O_5$
46.264	1.9608	15	471, 711	$Ba_4Ti_{13}O_{30}$
46.361	1.9569	20	-544, 073	$Ba_6Ti_{17}O_{40}$
46.553	1.9493	20	27-3	$Ba_6Ti_{17}O_{40}$
46.746	1.9417	25	115, 173+	$Ba_4Ti_{13}O_{30}$
47.225	1.9231	20	-671	$Ba_6Ti_{17}O_{40}$
47.225	1.9231	10	120	$BaTi_2O_5$
47.225	1.9231	25		$BaTi_4O_9$
47.225	1.9231	25		$Ba_2Ti_9O_{20}$
47.902	1.8975	5	642	$Ba_4Ti_{13}O_{30}$
47.999	1.8939	25		$BaTi_4O_9$
48.577	1.8727	10	524, 940	$Ba_6Ti_{17}O_{40}$
48.771	1.8657	35	931, 662	$Ba_6Ti_{17}O_{40}$
48.967	1.8587	50		$BaTi_5O_{11}$
48.967	1.8587	10		$BaTi_4O_9$
49.062	1.8553	40	504, 562	$Ba_4Ti_{13}O_{30}$
49.355	1.8450	15	215,-335+	$Ba_6Ti_{17}O_{40}$
49.645	1.8349	20	-804	$Ba_6Ti_{17}O_{40}$
49.645	1.8349	15	-504, 404	$BaTi_2O_5$
49.743	1.8315	10		$BaTi_4O_9$
49.938	1.8248	20		$BaTi_4O_9$
50.035	1.8215	35		$Ba_2Ti_9O_{20}$
50.425	1.8083	9	660,315	$Ba_4Ti_{13}O_{30}$
50.620	1.8018	15	235,291	$Ba_4Ti_{13}O_{30}$
50.620	1.8018	10	-222,315	$BaTi_2O_5$
50.620	1.8018	6	102	$BaTiO_3$
51.011	1.7889	8	201	$BaTiO_3$
51.109	1.7857	7	210	$BaTiO_3$
51.208	1.7825	20		$Ba_2Ti_9O_{20}$
51.303	1.7794	11	-582,-744	$Ba_6Ti_{17}O_{40}$
51.502	1.7730	10		$BaTi_4O_9$
51.794	1.7637	11	-862,680	$Ba_6Ti_{17}O_{40}$

TABLE 1 (cont.) : Xray Diffraction Data For Barium Titanate Phases

2θ(deg)	d(Å)	I/I_{max}	hkl	Phase
51.892	1.7606	11	-535	$Ba_6Ti_{17}O_{40}$
52.582	1.7391	45	202	Al_2O_3
52.877	1.7301	5	364	$Ba_4Ti_{13}O_{30}$
53.171	1.7212	11	811	$Ba_4Ti_{13}O_{30}$
53.568	1.7094	15	335	$Ba_6Ti_{17}O_{40}$
53.963	1.6978	7	544, 604	$Ba_4Ti_{13}O_{30}$
54.063	1.6949	25		$BaTi_4O_9$
54.260	1.6892	15	-513, -511	$BaTi_2O_5$
54.260	1.6892	15		$Ba_2Ti_9O_{20}$
54.361	1.6863	60	211	TiO_2
55.354	1.6584	10	2.10.0	$Ba_4Ti_{13}O_{30}$
55.455	1.6556	15	820, 831	$Ba_4Ti_{13}O_{30}$
55.653	1.6502	20		$BaTi_5O_{11}$
55.855	1.6447	20	435, 464+	$Ba_4Ti_{13}O_{30}$
55.955	1.6420	15	112	$BaTiO_3$
56.253	1.6340	35	211	$BaTiO_3$
56.653	1.6234	20	220	TiO_2
56.756	1.6207	10		$BaTi_4O_9$
57.056	1.6129	40		$Ba_2Ti_9O_{20}$
57.257	1.6077	15	515, 573+	$Ba_4Ti_{13}O_{30}$
57.359	1.6051	15	-324, 224	$BaTi_2O_5$
57.559	1.6000	80	116	Al_2O_3
57.559	1.6000	45		$Ba_2Ti_9O_{20}$
58.264	1.5823	30		$BaTi_4O_9$
58.467	1.5773	6	644	$Ba_4Ti_{13}O_{30}$
58.769	1.5699	25		$BaTi_4O_9$
59.175	1.5601	30	1.0.10	$BaTi_2O_5$
59.279	1.5576	25	704, 762	$Ba_4Ti_{13}O_{30}$
59.684	1.5480	10		$BaTi_4O_9$
59.786	1.5456	4		Al_2O_3
60.194	1.5361	20		$BaTi_4O_9$
60.806	1.5221	15		$Ba_2Ti_9O_{20}$
61.215	1.5129	6	122	Al_2O_3
61.318	1.5106	8	018	Al_2O_3
61.526	1.5060	15	513, 4.0.10	$BaTi_2O_5$
61.626	1.5038	15		$Ba_2Ti_9O_{20}$
61.936	1.4970	10		$BaTi_4O_9$
62.038	1.4948	15	-419	$BaTi_2O_5$
62.246	1.4903	10	420	$BaTi_2O_5$
62.761	1.4793	10	002	TiO_2
63.175	1.4706	25		$BaTi_5O_{11}$
64.006	1.4535	10		$BaTi_4O_9$
64.006	1.4535	10	210	TiO_2
64.633	1.4409	25		$Ba_2Ti_9O_{20}$
64.739	1.4388	25		$BaTi_5O_{11}$
65.156	1.4306	10	422	$BaTi_2O_5$
65.366	1.4265	30		$Ba_2Ti_9O_{20}$
65.470	1.4245	10	-2.1.11, 228	$BaTi_2O_5$
65.470	1.4245	2	221	TiO_2
65.787	1.4184	12	202	$BaTiO_3$
65.996	1.4144	25		$Ba_2Ti_9O_{20}$
66.102	1.4124	10	220	$BaTiO_3$
66.522	1.4045	30	124	Al_2O_3
67.051	1.3947	30	611	$BaTi_2O_5$
67.154	1.3928	35	-5.0.10	$BaTi_2O_5$
67.368	1.3889	35	417, -3.1.11	$BaTi_2O_5$
68.221	1.3736	50	030	Al_2O_3
68.221	1.3736	10	-328, 128	$BaTi_2O_5$
68.970	1.3605	20	301	TiO_2
69.290	1.3550	20		$Ba_2Ti_9O_{20}$

TABLE 1 (cont.) : Xray Diffraction Data For Barium Titanate Phases

2θ(deg)	d(Å)	I/I_{max}	hkl	Phase
69.501	1.3514	10		$BaTi_4O_9$
69.826	1.3459	12	112	TiO_2
70.040	1.3423	15	-524, 424	$BaTi_2O_5$
70.365	1.3369	2	125	Al_2O_3
70.365	1.3369	5	212	$BaTiO_3$
70.687	1.3316	2	221	$BaTiO_3$
71.446	1.3193	15		$Ba_2Ti_9O_{20}$
72.429	1.3038	2	311	TiO_2
74.302	1.2755	4	208	Al_2O_3
74.302	1.2755	5	103	$BaTiO_3$
75.080	1.2642	7	301	$BaTiO_3$
75.192	1.2626	9	310	$BaTiO_3$
76.199	1.2484	20		$BaTi_4O_9$
76.532	1.2438	4	202	TiO_2
76.868	1.2392	15	1.0.10	Al_2O_3
77.207	1.2346	8	119	Al_2O_3
78.001	1.2240	10	330	$BaTi_4O_9$
78.799	1.2136	3	113	$BaTiO_3$
78.915	1.2121	20		$BaTi_4O_9$
79.488	1.2048	5	311	$BaTiO_3$
79.830	1.2005	2	212	TiO_2
80.637	1.1905	10		$BaTi_4O_9$
80.752	1.1891	8	220	Al_2O_3
80.990	1.1862	15	-626	$BaTi_2O_5$
81.222	1.1834	10	3.1.11	$BaTi_2O_5$
82.387	1.1696	6	321	TiO_2
83.097	1.1614	10	6.1.11, -7.0.10	$BaTi_2O_5$
83.210	1.1601	1	306	Al_2O_3
83.333	1.1587	10		$BaTi_4O_9$
83.448	1.1574	7	222	$BaTiO_3$
84.278	1.1481	4	400	TiO_2
84.396	1.1468	6	223	Al_2O_3
85.230	1.1377	2	311	Al_2O_3
86.321	1.1261	6	312	Al_2O_3
86.560	1.1236	4	128	Al_2O_3
87.043	1.1186	1	203	$BaTiO_3$
87.287	1.1161	1	302	$BaTiO_3$
87.533	1.1136	20		$BaTi_4O_9$
87.533	1.1136	2	410	TiO_2
88.149	1.1074	1	320	$BaTiO_3$
89.134	1.0977	8	0.2.10	Al_2O_3
89.506	1.0941	8	222	TiO_2
90.663	1.0834	4	0.0.12	Al_2O_3
90.633	1.0834	4	330	TiO_2
91.258	1.0776	8	134	Al_2O_3
91.509	1.0753	7	213	$BaTiO_3$
92.149	1.0695	12	312	$BaTiO_3$
92.272	1.0684	12	321	$BaTiO_3$
95.372	1.0417	15	226	Al_2O_3
95.372	1.0417	6	411	TiO_2
96.030	1.0363	6	312	TiO_2
97.227	1.0267	4	420	TiO_2
98.436	1.0173	2	402	Al_2O_3
99.521	1.0091	1	004	$BaTiO_3$

Table 2: Peaks Selected for Phase Identification and Quantitative Analysis

Phase	2θ(degrees)	d(Å)	hkl	I/I_{max} (%)	
$BaTiO_3$	92.149	1.0695	312	12	QA†
	92.272	1.0684	321	12	QA
$Ba_6Ti_{17}O_{40}$	34.503	2.5974	451	20	QA
$Ba_4Ti_{13}O_{30}$	19.066	4.6512	102, 131	25	
	20.769	4.2735	022, 040	60	QA
$BaTi_4O_9$	18.619	4.7619	021	15	
	23.197	3.8314	031	40	QA
$Ba_2Ti_9O_{20}$	60.806	1.5221	---	15	
	71.446	1.3193	---	15	
$BaTi_5O_{11}$	17.189	5.1546	120	10	
	63.175	1.4706	---	25	
TiO_2	36.077	2.4876	101	50	QA
	62.761	1.4793	002	10	QA
Al_2O_3	37.752	2.3810	110	40	QA
	52.556	1.7399	024	42	QA

†Denotes peaks which are used for quantitative analysis.

Table 3: Properties of Raw Materials

Material	TiO_2 (Rutile)	$BaTiO_3$	Al_2O_3
Manufacturer	Johnson Mathey Co. Puratronic Grade	Johnson Mathey Co. Puratronic Grade	Baker Chemical Co. Reagent Grade
Batch No.	S94967C	S93020C	106177
Manufacturers Listed Impurities	Ca 10 ppm Mg 2 ppm Si 5 ppm Ag 1 ppm	Si 10 ppm Mg 1 ppm Ca < 1 ppm	Cl 0.002 % SO_4 < 0.003 % Pb < 0.0005 % Fe < 0.02 %
Largest Particle Size (SEM)	< 80 μm	< 40 μm	< 75 μm
Surface Area (BET)	1.3 m^2/g	2.7 m^2/g	---
Equivalent Spherical Radius (BET)	0.53μm	0.29μm	---

Table 4: Summary of Samples

Sample ID	Time at 1050°C	Weight Fraction Al_2O_3†
Sraw	Unfired	0.2982
S24M	0.4 Hr	0.3001
S01H	1 Hr	0.3001
S02H	2 Hr	0.3003
S08H	8 Hr	0.3001
S24H	24 Hr	0.2999
S48H	48 Hr	0.3000
S06D	144 Hr	0.3000

†Added after reaction as standard for quantitative analysis.

Table 5a: Results of IDR Peak Search for Sample Sraw

Peak	2θ(deg)	d-spacing	Intensity	FWHM	Phase	hkl	2θ(deg)
1	22.147	4.0106	14235	0.421	$BaTiO_3$	001, 100	22.208
2	23.942	3.7138	1137	0.527	?		
3	25.589	3.4784	3890	0.200	Al_2O_3	210	25.545
4	27.439	3.2479	19231	0.227	TiO_2	110	27.448
5	31.529	2.8353	72521	0.360	$BaTiO_3$	101,110	31.506
6	35.152	2.5509	6219	0.200	Al_2O_3	104	35.151
7	36.075	2.4877	8710	0.220	TiO_2	101	36.077
8	37.791	2.3786	2747	0.232	Al_2O_3	110	37.752
9	38.885	2.3142	19779	0.309	$BaTiO_3$	111	38.874
10	41.246	2.1870	4241	0.232	TiO_2	111	41.222
11	43.376	2.0844	6561	0.215	Al_2O_3	113	43.400
12	44.090	2.0523	1053	0.194	TiO_2	210	44.065
13	45.332	1.9989	23556	0.598	$BaTiO_3$	200	45.402
14	50.972	1.7902	6649	0.612	$BaTiO_3$	201, 210	51.057
15	52.572	1.7394	3211	0.238	Al_2O_3	202	52.582
16	54.341	1.6869	12073	0.274	TiO_2	211	54.361
17	56.238	1.6344	26911	0.581	$BaTiO_3$	211	56.253
18	57.527	1.6008	7427	0.268	Al_2O_3	116	57.559
19	61.305	1.5109	1065	0.367	Al_2O_3	122, 018	61.274
20	62.775	1.4790	1581	0.256	TiO_2	002	62.761
21	64.095	1.4517	1613	0.269	TiO_2	210	64.006
22	65.881	1.4166	12462	0.630	$BaTiO_3$	202, 220	65.930
23	66.522	1.4045	2912	0.288	Al_2O_3	124	66.522
24	68.226	1.3735	4070	0.315	Al_2O_3	030	68.221
25	69.045	1.3592	2983	0.226	TiO_2	301	68.970
26	69.820	1.3460	1521	0.227	TiO_2	112	69.826
27	70.456	1.3354	3034	0.544	Al_2O_3	125	70.365
					$BaTiO_3$	212, 221	70.457
28	75.067	1.2644	10369	0.925	$BaTiO_3$	301, 310	75.143
29	76.875	1.2391	2422	0.503	Al_2O_3	1.0.10	76.868
30	79.393	1.2060	4521	0.824	$BaTiO_3$	113, 311	79.230
31	80.670	1.1901	742	0.401	Al_2O_3	220	80.752
32	82.369	1.1698	1071	0.349	TiO_2	321	82.387
33	83.483	1.1570	3113	0.453	$BaTiO_3$	222	83.448
34	87.780	1.1111	1416	0.792	TiO_2	410	87.533
35	89.547	1.0937	1386	0.309	TiO_2	222	89.506
36	90.740	1.0824	751	0.236	Al_2O_30	00.12	90.663
					TiO_2	330	90.633
37	92.027	1.0706	12970	1.027	$BaTiO_3$	312, 321	92.211
38	95.263	1.0426	2736	0.421	Al_2O_3	226	95.372
					TiO_2	411	95.372

Table 5b: Results of IDR Peak Search for Sample S24M

Peak	2θ(deg)	d-spacing	Intensity	FWHM	Phase	hkl	2θ(deg)
1					$BaTi_4O_9$	021	18.619
2					$Ba_4Ti_{13}O_{30}$	102, 131	19.066
3					$Ba_4Ti_{13}O_{30}$	022, 040	20.769
4	22.254	3.9916	12810	0.378	$BaTiO_3$	001, 100	22.208
5	25.647	3.4706	3953	0.217	Al_2O_3	210	25.545
6	27.523	3.2382	18726	0.202	$Ba_4Ti_{13}O_{30}$	411	27.448
					TiO_2	110	27.448
7	28.410	3.1391	1131	0.236	$Ba_4Ti_{13}O_{30}$	322, 113	28.267
					$BaTi_4O_9$	002, 041	28.358
8	29.995	2.9767	1253	0.287	$BaTi_4O_9$	130, 121	30.000
9	31.616	2.8277	68432	0.337	$BaTiO_3$	101, 110	31.506
10	34.031	2.6323	870	0.315	$Ba_4Ti_{13}O_{30}$	260	33.949
					$BaTi_4O_9$	032, 051	33.949
11	35.245	2.5444	6775	0.206	Al_2O_3	104	35.151
12	36.167	2.4816	7684	0.194	TiO_2	101	36.077
13	37.886	2.3729	2520	0.234	Al_2O_3	110	37.752
14	38.971	2.3093	17843	0.290	$BaTiO_3$	111	38.874
					$BaTi_4O_9$	122, 150	39.062
15	41.323	2.1831	3835	0.200	TiO_2	111	41.222
					$Ba_4Ti_{13}O_{30}$	304, 362	41.412
16	43.440	2.0815	7343	0.241	Al_2O_3	113	43.400
17	44.153	2.0495	793	0.172	$Ba_4Ti_{13}O_{30}$	640	44.065
					TiO_2	210	44.065
18	45.416	1.9954	21068	0.569	$Ba_4Ti_{13}O_{30}$	533	45.306
					$BaTiO_3$	200	45.402
19	51.057	1.7874	6210	0.587	$BaTiO_3$	201, 210	51.057
20	52.654	1.7369	2930	0.226	Al_2O_3	202	52.582
21	54.421	1.6846	11804	0.250	TiO_2	211	54.361
22	56.309	1.6325	25385	0.546	$BaTiO_3$	211	56.253
23	57.614	1.5986	7177	0.277	Al_2O_3	116	57.559
24	61.390	1.5090	811	0.312	Al_2O_3	122, 018	61.274
25	62.818	1.4781	1601	0.259	TiO_2	002	62.761
26	64.174	1.4501	1670	0.265	TiO_2	210	64.006
					$BaTi_4O_9$	202, 220	64.006
27	65.939	1.4155	11680	0.620	$BaTiO_3$		65.930
28	66.597	1.4031	2699	0.274	Al_2O_3	124	66.522
29	68.289	1.3724	3684	0.282	Al_2O_3	030	68.221
30	69.097	1.3583	3027	0.238	TiO_2	301	68.970
31	69.850	1.3455	1809	0.236	TiO_2	112	69.826
32	70.553	1.3338	3060	0.556	Al_2O_3	125	70.365
					$BaTiO_3$	212, 221	70.457
33	75.164	1.2630	9721	0.918	$BaTiO_3$	301, 310	75.143
34					$BaTi_4O_9$	330	78.001
35	79.480	1.2049	4584	0.824	$BaTiO_3$	113, 311	79.230
36	83.545	1.1563	3180	0.444	$BaTiO_3$	222	83.448
37	84.387	1.1469	1002	0.388	TiO_2	400	84.278
					Al_2O_3	223	84.396
38	89.599	1.0932	945	0.164	TiO_2	222	89.506
39	90.815	1.0817	858	0.260	Al_2O_3	0.0.12	90.663
					TiO_2	330	90.633
40	92.094	1.0700	11568	0.921	$BaTiO_3$	312, 321	92.211
41	95.323	1.0421	2790	0.426	Al_2O_3	226	95.372
					TiO_2	411	95.372
42	97.278	1.0263	710	0.486	TiO_2	420	97.227

Table 5c: Results of IDR Peak Search for Sample S01H

Peak	2θ(deg)	d-spacing	Intensity	FWHM	Phase	hkl	2θ(deg)
1					$BaTi_4O_9$	021	18.619
2					$Ba_4Ti_{13}O_{30}$	102, 131	19.066
3					$Ba_4Ti_{13}O_{30}$	022, 040	20.769
4	22.148	4.0104	10401	0.364	$BaTiO_3$	001, 100	22.208
5	25.583	3.4791	3532	0.223	Al_2O_3	210	25.545
6	27.440	3.2478	18952	0.191	$Ba_4Ti_{13}O_{30}$	411	27.448
					TiO_2	110	27.448
7	28.322	3.1486	1918	0.284	$Ba_4Ti_{13}O_{30}$	322, 113	28.267
					$BaTi_4O_9$	002, 041	28.358
8	30.025	2.9738	2512	0.373	$BaTi_4O_9$	130, 121	30.000
9	31.532	2.8350	57658	0.348	$BaTiO_3$	101, 110	31.506
10	33.942	2.6390	1186	0.336	$Ba_4Ti_{13}O_{30}$	260	33.949
					$BaTi_4O_9$	032, 051	33.949
11	35.161	2.5503	5925	0.221	Al_2O_3	104	35.151
12	36.086	2.4870	7503	0.199	TiO_2	101	36.077
13	37.796	2.3783	2448	0.232	Al_2O_3	110	37.752
14	38.892	2.3138	15676	0.292	$BaTiO_3$	111	38.874
					$BaTi_4O_9$	122, 150	39.062
15	41.254	2.1866	4046	0.201	TiO_2	111	41.222
					$Ba_4Ti_{13}O_{30}$	304, 362	41.412
16	43.372	2.0846	6496	0.240	Al_2O_3	113	43.400
17	44.088	2.0524	1047	0.202	$Ba_4Ti_{13}O_{30}$	640	44.065
					TiO_2	210	44.065
18	45.335	1.9988	20599	0.599	$Ba_4Ti_{13}O_{30}$	533	45.306
					$BaTiO_3$	200	45.402
19	47.891	1.8979	655	0.307	$Ba_4Ti_{13}O_{30}$	642	47.902
					$BaTi_4O_9$		47.999
20	50.975	1.7901	5278	0.534	$BaTiO_3$	201, 210	51.057
21	52.575	1.7393	3032	0.254	Al_2O_3	202	52.582
22	54.341	1.6869	11774	0.253	TiO_2	211	54.361
23	56.234	1.6345	20396	0.490	$BaTiO_3$	211	56.253
24	56.642	1.6237	3895	0.215	TiO_2	220	56.653
					$BaTi_4O_9$		56.756
25	57.535	1.6006	5700	0.245	Al_2O_3	116	57.559
26	61.314	1.5107	687	0.259	Al_2O_3	122, 018	61.274
27	62.737	1.4798	1572	0.255	TiO_2	002	62.761
28	64.095	1.4517	1747	0.279	TiO_2	210	64.006
					$BaTi_4O_9$	202, 220	64.006
29	65.860	1.4170	11095	0.637	$BaTiO_3$	124	65.930
30	66.522	1.4045	2712	0.273	Al_2O_3		66.522
31	68.209	1.3738	3284	0.256	Al_2O_3	030	68.221
32	69.016	1.3597	2966	0.255	TiO_2	301	68.970
33	69.802	1.3463	1501	0.230	TiO_2	112	69.826
34	70.462	1.3353	2673	0.549	Al_2O_3	125	70.365
					$BaTiO_3$	212, 221	70.457
35	75.080	1.2642	8975	0.860	$BaTiO_3$	301, 310	75.143
36					$BaTi_4O_9$	330	78.001
37	79.401	1.2059	4265	0.812	$BaTiO_3$	113, 311	79.230
38	82.369	1.1698	994	0.343	TiO_2	321	82.387
39	83.492	1.1569	2787	0.441	$BaTi_4O_9$		83.333
					$BaTiO_3$	222	83.448
40	84.288	1.1480	1230	0.450	TiO_2	400	84.278
					Al_2O_3	223	84.396
41	86.397	1.1253	711	0.584	Al_2O_3	312, 128	86.417
42	87.592	1.1130	1119	0.832	$BaTi_4O_9$		87.533
					TiO_2	410	87.533
43	89.516	1.0940	1259	0.260	TiO_2	222	89.506
44	90.740	1.0824	711	0.256	Al_2O_3	0.0.12	90.663
					TiO_2	330	90.633
45	92.038	1.0705	10483	0.921	$BaTiO_3$	312, 321	92.211
46	95.275	1.0425	2802	0.454	Al_2O_3	226	95.372
					TiO_2	411	95.372
47	97.215	1.0268	757	0.429	TiO_2	420	97.227

Table 5d: Results of IDR Peak Search for Sample S02H

Peak	2θ(deg)	d-spacing	Intensity	FWHM	Phase	hkl	2θ(deg)
1					$BaTi_4O_9$	021	18.619
2					$Ba_4Ti_{13}O_{30}$	102, 131	19.066
3					$Ba_4Ti_{13}O_{30}$	022, 040	20.769
4	22.182	4.0043	10798	0.371	$Ba_4Ti_{13}O_{30}$	231	22.026
5	23.169	3.8359	843	0.248	$BaTiO_3$	001, 100	22.208
					$BaTi_4O_9$	031	23.197
6	25.587	3.4786	3768	0.200	Al_2O_3	210	25.545
7	27.461	3.2453	18697	0201	$Ba_4Ti_{13}O_{30}$	411	27.448
					TiO_2	110	27.448
8	28.343	3.1463	1733	0.224	$Ba_4Ti_{13}O_{30}$	322, 113	28.267
					$BaTi_4O_9$	002, 041	28.358
9	29.914	2.9846	1284	0.206	$BaTi_4O_9$	130, 121	30.000
10	30.099	2.9666	1659	0.168	$BaTi_4O_9$	130, 121	30.000
11	31.549	2.8335	59109	0.333	$BaTiO_3$	101, 110	31.506
12	33.953	2.6382	1269	0.189	$Ba_4Ti_{13}O_{30}$	260	33.949
					$BaTi_4O_9$	032, 051	33.949
13	35.168	2.5498	6228	0.218	Al_2O_3	104	35.151
14	36.087	2.4869	7793	0.193	TiO_2	101	36.077
15	37.795	2.3784	2696	0.200	Al_2O_3	110	37.752
16	38.911	2.3127	16175	0.291	$BaTiO_3$	111	38.874
					$BaTi_4O_9$	122, 150	39.062
17	41.262	2.1862	4070	0.220	TiO_2	111	41.222
					$Ba_4Ti_{13}O_{30}$	304, 362	41.412
18	43.374	2.0845	6930	0.223	Al_2O_3	113	43.400
19	44.074	2.0530	1169	0.165	$Ba_4Ti_{13}O_{30}$	640	44.065
					TiO_2	210	44.065
20	45.376	1.9971	19097	0.573	$Ba_4Ti_{13}O_{30}$	533	45.306
					$BaTiO_3$	200	45.402
21	47.883	1.8982	733	0.211	$Ba_4Ti_{13}O_{30}$	642	47.902
					$BaTi_4O_9$	201, 210	47.999
22	51.002	1.7892	5709	0.574	$BaTiO_3$		51.057
23	52.585	1.7390	3260	0.251	Al_2O_3	202	52.582
24	54.375	1.6859	11334	0.252	TiO_2	211	54.361
25	56.242	1.6343	20188	0.472	$BaTiO_3$	211	56.253
26	56.680	1.6227	3978	0.225	TiO_2	220	56.653
					$BaTi_4O_9$		56.756
27	57.539	1.6005	6384	0.251	Al_2O_3	116	57.559
28	60.009	1.5404	681	0.332	$BaTi_4O_9$		60.194
29	61.318	1.5106	712	0.277	Al_2O_3	122, 018	61.274
30	62.770	1.4791	1581	0.248	TiO_2	002	62.761
31	64.095	1.4517	1741	0.301	$BaTi_4O_9$		64.006
					TiO_2	210	64.006
32	65.855	1.4171	11106	0.624	$BaTiO_3$	202, 220	65.930
33	66.522	1.4045	2900	0.277	Al_2O_3	124	66.522
34	68.221	1.3736	4025	0.312	Al_2O_3	030	68.221
35	69.051	1.3591	2951	0.228	TiO_2	301	68.970
36	69.814	1.3461	1454	0.209	TiO_2	112	69.826
37	70.462	1.3353	2692	0.531	Al_2O_3	125	70.365
					$BaTiO_3$	212, 221	70.457
38	75.108	1.2638	8949	0.852	$BaTiO_3$	301, 310	75.143
39	76.882	1.2390	1321	0.273	Al_2O_3	1.0.10	76.868
40					$BaTi_4O_9$	330	78.001
41	79.401	1.2059	4176	0.748	$BaTiO_3$	113, 311	79.230
42	83.510	1.1567	2955	0.445	$BaTi_4O_9$		83.333
					$BaTiO_3$	222	83.448
43	84.351	1.1473	889	0.323	TiO_2	400	84.278
					Al_2O_3	223	84.396
44	89.537	1.0938	808	0.148	TiO_2	222	89.506
45	90.772	1.0821	877	0.264	Al_2O_3	0.0.12	90.663
					TiO_2	330	90.633
46	92.094	1.0700	10957	0.908	$BaTiO_3$	312, 321	92.210
47	95.287	1.0424	1750	0.264	Al_2O_3	226	95.372
					TiO_2	411	95.372

Table 5e: Results of IDR Peak Search for Sample S08H

Peak	2θ(deg)	d-spacing	Intensity	FWHM	Phase	hkl	2θ(deg)
1					$BaTi_4O_9$	021	18.619
2					$Ba_4Ti_{13}O_{30}$	102, 131	19.066
3	20.822	4.2626	813	0.199	$Ba_4Ti_{13}O_{30}$	022, 040	20.769
4	22.170	4.0064	11966	0.423	$Ba_4Ti_{13}O_{30}$	231	22.026
					$BaTiO_3$	001, 100	22.208
5	23.154	3.8384	939	0.187	$BaTi_4O_9$	031	23.197
6	25.599	3.4770	4388	0.212	Al_2O_3	210	25.545
7	27.473	3.2440	17215	0.198	$Ba_4Ti_{13}O_{30}$	411	27.448
					TiO_2	110	27.448
8	28.350	3.1456	3322	0.210	$Ba_4Ti_{13}O_{30}$	322, 113	28.267
					$BaTi_4O_9$	002, 041	28.358
					$Ba_2Ti_9O_{20}$	130, 121	28.449
9	29.992	2.9843	4662	0.225	$BaTi_4O_9$		30.000
					$Ba_2Ti_9O_{20}$		30.000
10	31.561	2.8325	56969	0.330	$BaTiO_3$	101, 110	31.506
11	33.721	2.6558	1063	0.233	$Ba_2Ti_9O_{20}$		33.579
					$Ba_4Ti_{13}O_{30}$	313, 342	33.672
12	33.962	2.6375	1690	0.192	$Ba_4Ti_{13}O_{30}$	260	33.949
					$BaTi_4O_9$	032, 051	33.949
13	35.175	2.5493	6286	0.206	Al_2O_3	104	35.151
14	36.107	2.4856	6736	0.209	TiO_2	101	36.077
15	37.803	2.3779	2864	0.232	Al_2O_3	110	37.752
16	38.916	2.3124	16047	0.292	$BaTiO_3$	111	38.874
					$BaTi_4O_9$	122, 150	39.062
17	41.280	2.1853	4194	0.250	TiO_2	111	41.222
					$Ba_4Ti_{13}O_{30}$	304, 362	41.412
18	43.387	2.0839	6623	0.225	Al_2O_3	113	43.400
19	44.079	2.0528	1151	0.188	$Ba_4Ti_{13}O_{30}$	640	44.065
					TiO_2	210	44.065
20	45.371	1.9973	19156	0.592	$Ba_4Ti_{13}O_{30}$	533	45.306
					$BaTiO_3$	200	45.402
21	47.899	1.8976	1035	0.200	$Ba_4Ti_{13}O_{30}$	642	47.902
					$BaTi_4O_9$	201, 210	47.999
22	51.002	1.7892	5845	0.608	$BaTiO_3$		51.057
23	52.588	1.7389	3309	0.279	Al_2O_3	202	52.582
24	54.375	1.6859	10062	0.231	$Ba_2Ti_9O_{20}$		54.260
					TiO_2	211	54.361
25	56.264	1.6337	20590	0.485	$BaTiO_3$	211	56.253
26	56.680	1.6227	3437	0.198	TiO_2	220	56.653
					$BaTi_4O_9$		56.756
27	57.539	1.6005	6473	0.241	Al_2O_3	116	57.559
					$Ba_2Ti_9O_{20}$		57.559
28	60.013	1.5403	745	0.279	$BaTi_4O_9$		60.194
29					$Ba_2Ti_9O_{20}$	122, 018	60.806
30	61.332	1.5103	676	0.246	Al_2O_3		61.274
31	62.775	1.4790	1433	0.267	TiO_2	002	62.761
32	64.129	1.4510	1816	0.366	$BaTi_4O_9$		64.006
					TiO_2	210	64.006
33	65.844	1.4173	10834	0.597	$BaTiO_3$	202, 220	65.930
					$Ba_2Ti_9O_{20}$		65.996
34	66.559	1.4038	3188	0.314	Al_2O_3	124	66.522
35	68.249	1.3731	3807	0.272	Al_2O_3	030	68.221
36	69.051	1.3591	2492	0.230	TiO_2	301	68.970
37	69.808	1.3462	853	0.137	TiO_2	112	69.826
38	70.517	1.3344	2689	0.512	Al_2O_3	125	70.365
					$BaTiO_3$	212, 221	70.457
39					$Ba_2Ti_9O_{20}$		71.446
40	75.094	1.2640	4966	0.525	$BaTiO_3$	301, 310	75.143
41	76.919	1.2385	1392	0.298	Al_2O_3	1.0.10	76.868
42					$BaTi_4O_9$	330	78.001
43	79.048	1.2104	874	0.291	$BaTi_4O_9$		78.915

Table 5e: Results of IDR Peak Search for Sample S08H (cont.)

44	79.417	1.2057	2448	0.463	$BaTiO_3$	113, 311	79.230
45	83.501	1.1568	3131	0.475	$BaTi_4O_9$		83.333
					$BaTiO_3$	222	83.448
46	84.324	1.1476	1212	0.469	TiO_2	400	84.278
					Al_2O_3	223	84.396
47	87.760	1.1113	1356	0.524			
48	89.568	1.0935	847	0.157	TiO_2	222	89.506
49	90.772	1.0821	985	0.269	Al_2O_3	0.0.12	90.663
					TiO_2	330	90.633
50	92.027	1.0706	9812	0.853	$BaTiO_3$	312, 321	92.210
51	95.287	1.0424	1592	0.251	Al_2O_3	226	95.372
					TiO_2	411	95.372

Table 5f: Results of IDR Peak Search for Sample S24H

Peak	2θ(deg)	d-spacing	Intensity	FWHM	Phase	hkl	2θ(deg)
1					$BaTi_4O_9$	021	18.619
2					$Ba_4Ti_{13}O_{30}$	102, 131	19.066
3					$Ba_4Ti_{13}O_{30}$	022, 040	20.769
4	22.207	3.9999	15085	0.604	$Ba_4Ti_{13}O_{30}$	231	22.026
					$BaTiO_3$	001, 100	22.208
5	25.620	3.4742	5161	0.265	Al_2O_3	210	25.545
6	27.464	3.2459	5210	0.236	$Ba_4Ti_{13}O_{30}$	411	27.448
					TiO_2	110	27.448
7	30.093	2.9672	7393	0.382	$BaTi_4O_9$	130, 121	30.000
					$Ba_2Ti_9O_{20}$		30.000
8	31.555	2.8330	52989	0.373	$BaTiO_3$	101, 110	31.506
9	35.145	2.5514	6576	0.217	Al_2O_3	104	35.151
10					TiO_2	101	36.077
11	37.803	2.3779	2774	0.229	Al_2O_3	110	37.752
12	38.925	2.3119	13837	0.312	$BaTiO_3$	111	38.874
					$BaTi_4O_9$	122, 150	39.062
13	41.266	2.1860	5789	0.304	TiO_2	111	41.222
					$Ba_4Ti_{13}O_{30}$	304, 362	41.412
14	43.354	2.0854	7193	0.260	Al_2O_3	113	43.400
15	44.083	2.0526	2110	0.252	$Ba_4Ti_{13}O_{30}$	640	44.065
					TiO_2	210	44.065
16	45.277	2.0012	18180	0.633	$Ba_4Ti_{13}O_{30}$	533	45.306
					$BaTiO_3$	200	45.402
17	49.105	1.8538	1249	0.416	$BaTi_4O_9$	504, 562	48.967
					$Ba_4Ti_{13}O_{30}$	201, 210	49.062
18	50.978	1.7900	5965	0.742	$BaTiO_3$		51.057
19	52.592	1.7388	2935	0.271	Al_2O_3	202	52.582
20	54.361	1.6863	10576	0.234	$Ba_2Ti_9O_{20}$		54.260
					TiO_2	211	54.361
21	56.249	1.6341	20869	0.592	$BaTiO_3$	211	56.253
22	57.527	1.6008	5793	0.232	Al_2O_3	116	57.559
					$Ba_2Ti_9O_{20}$		57.559
23	58.519	1.5760	651	0.379	$Ba_4Ti_{13}O_{30}$	644	58.467
24	60.009	1.5404	1045	0.332	$BaTi_4O_9$		60.194
25					$Ba_2Ti_9O_{20}$		60.806
26	61.318	1.5106	637	0.254	Al_2O_3	122, 018	61.274
27	62.761	1.4793	1436	0.250	TiO_2	002	62.761
28	64.095	1.4517	1905	0.280	$BaTi_4O_9$		64.006
					TiO_2	210	64.006
29	65.886	1.4165	9179	0.680	$BaTiO_3$	202, 220	65.930
					$Ba_2Ti_9O_{20}$	124	65.996
30	66.522	1.4045	3604	0.353	Al_2O_3		66.522
31	68.260	1.3729	3667	0.296	Al_2O_3	030	68.221
32	69.068	1.3588	2455	0.218	TiO_2	301	68.970
33	69.832	1.3458	1400	0.219	TiO_2	112	69.826
34					$Ba_2Ti_9O_{20}$		71.446
35	75.060	1.2645	7920	0.967	$BaTiO_3$	301, 310	75.143
36	76.912	1.2386	2318	0.536	Al_2O_3	1.0.10	76.868
37					$BaTi_4O_9$	330	78.001
38	79.378	1.2062	3496	0.846	$BaTiO_3$	113, 311	79.230
39	80.727	1.1894	967	0.504	$BaTi_4O_9$		80.637
					Al_2O_3	220	80.752
40	82.438	1.1690	1037	0.375	TiO_2	321	82.387
41	83.536	1.1564	1805	0.423	$BaTiO_3$	222	83.448
42	87.582	1.1131	1075	0.759	$BaTi_4O_9$		87.533
					TiO_2	410	87.533
43	89.578	1.0934	1695	0.472	TiO_2	222	89.506
44	92.082	1.0701	10365	1.056	$BaTiO_3$	312, 321	92.210
45	95.299	1.0423	3002	0.462	Al_2O_3	226	95.372
					TiO_2	411	95.372
46	97.278	1.0263	771	0.482	TiO_2	420	97.227

Table 5g: Results of IDR Peak Search for Sample S48H

Peak	2θ(deg)	d-spacing	Intensity	FWHM	Phase	hkl	2θ(deg)
1	18.641	4.7562	595	0.209	$BaTi_4O_9$	021	18.619
2	19.076	4.6487	798	0.246	$Ba_4Ti_{13}O_{30}$	102, 131	19.066
3	20.802	4.2667	1401	0.170	$Ba_4Ti_{13}O_{30}$	022, 040	20.769
4	22.158	4.0086	8576	0.401	$Ba_4Ti_{13}O_{30}$	231	22.026
					$BaTiO_3$	001, 100	22.208
5	23.154	3.8383	1441	0.210	$BaTi_4O_9$	031	23.197
6	25.589	3.4783	5021	0.233	Al_2O_3	210	25.545
7	26.224	3.3956	687	0.192	$Ba_4Ti_{13}O_{30}$	302	26.178
					$Ba_2Ti_9O_{20}$	411	26.269
8	27.462	3.2452	17204	0.202	$Ba_4Ti_{13}O_{30}$	110	27.448
					TiO_2		27.448
9	28.345	3.1461	5788	0.221	$Ba_4Ti_{13}O_{30}$	322, 113	28.267
					$BaTi_4O_9$	002, 041	28.358
					$Ba_2Ti_9O_{20}$	130, 121	28.449
10	29.900	2.9859	3232	0.230	$BaTi_4O_9$		30.000
					$Ba_2Ti_9O_{20}$		30.000
11	30.467	2.9316	549	0.158	Ba6Ti17O40	242	30.274
					$Ba_4Ti_{13}O_{30}$	213, 242	30.457
12	31.547	2.8337	44730	0.344	$BaTiO_3$	101, 110	31.506
13	32.040	2.7912	2094	0.212	$Ba_4Ti_{13}O_{30}$	133	32.015
					$Ba_2Ti_9O_{20}$		32.015
14	33.712	2.6565	2373	0.249	$Ba_2Ti_9O_{20}$		33.579
					$Ba_4Ti_{13}O_{30}$	313, 342	33.672
15	33.960	2.6377	2004	0.169	$Ba_4Ti_{13}O_{30}$	260	33.949
					$BaTi_4O_9$	032, 051	33.949
16	35.166	2.5499	6694	0.212	Al_2O_3	104	35.151
17	36.090	2.4867	6011	0.186	TiO_2	101	36.077
18	37.099	2.4214	476	0.178	$BaTi_4O_9$	102, 060	37.100
					$Ba_2Ti_9O_{20}$	110	37.287
19	37.796	2.3783	2976	0.230	Al_2O_3	111	37.752
20	38.913	2.3126	13381	0.315	$BaTiO_3$	122, 150	38.874
					$BaTi_4O_9$		39.062
21	41.289	2.1848	4763	0.281	TiO_2	111	41.222
					$Ba_4Ti_{13}O_{30}$	304, 362	41.412
22	41.640	2.1672	763	0.197	Al_2O_3	006	41.695
					$BaTi_4O_9$	132, 151	41.790
23	42.760	2.1130	575	0.274	$Ba_4Ti_{13}O_{30}$	602, 324	42.735
24	43.376	2.0844	6461	0.221	Al_2O_3	113	43.400
25	44.074	2.0530	1328	0.196	$Ba_4Ti_{13}O_{30}$	640	44.065
					TiO_2	210	44.160
26	44.988	2.0134	6495	0.366	$Ba_4Ti_{13}O_{30}$		44.924
					$BaTi_4O_9$	404, 462	45.019
27	45.352	1.9981	8920	0.340	$Ba_4Ti_{13}O_{30}$	533	45.306
					$BaTiO_3$	200	45.402
28	46.192	1.9637	595	0.218	Al_2O_3	202	46.169
					$Ba_4Ti_{13}O_{30}$	471, 711	46.264
29	46.782	1.9403	707	0.226	$Ba_4Ti_{13}O_{30}$	115, 173	46.746
30	47.204	1.9239	459	0.244	$BaTi_4O_9$		47.225
					$Ba_2Ti_9O_{20}$	642	47.225
31	47.889	1.8980	1418	0.240	$Ba_4Ti_{13}O_{30}$		47.902
					$BaTi_4O_9$	504,562	47.999
32	49.113	1.8535	1554	0.339	$BaTi_4O_9$		48.967
					$Ba_4Ti_{13}O_{30}$		49.062
33	50.173	1.8168	624	0.231	$Ba_2Ti_9O_{20}$		50.035
34	51.048	1.7877	3928	0.338	$BaTiO_3$	201, 210	51.057
					$Ba_2Ti_9O_{20}$	202	51.208
35	52.572	1.7394	3458	0.273	Al_2O_3	544,604	52.582
36	53.881	1.7002	518	0.169	$Ba_4Ti_{13}O_{30}$		53.963
					$BaTi_4O_9$		54.063

Table 5g: Results of IDR Peak Search for Sample S48H (cont.)

37	54.348	1.6867	5265	0.146	$Ba_2Ti_9O_{20}$		54.260
					TiO_2	211	54.361
38	56.253	1.6340	16573	0.490	$BaTiO_3$	211	56.253
39	56.642	1.6237	3709	0.231	TiO_2	220	56.653
					$BaTi_4O_9$		56.756
40	57.515	1.6011	6506	0.251	Al_2O_3	116	57.559
					$Ba_2Ti_9O_{20}$	704, 762	57.559
41	59.317	1.5567	622	0.203	$Ba_4Ti_{13}O_{30}$		59.279
42					$Ba_2Ti_9O_{20}$	122, 018	60.806
43	61.309	1.5108	574	0.236	Al_2O_3		61.274
44	61.941	1.4969	615	0.329	$BaTi_4O_9$		61.936
45	62.747	1.4796	661	0.139	TiO_2	002	62.761
46	64.085	1.4519	832	0.195	$BaTi_4O_9$		64.006
					TiO_2	210	64.006
47	65.787	1.4184	3296	0.275	$BaTiO_3$	202, 220	65.930
48	66.522	1.4045	3144	0.288	Al_2O_3	124	66.522
49	68.221	1.3736	2053	0.170	Al_2O_3	030	68.221
50	69.028	1.3595	1557	0.157	TiO_2	301	68.970
51	69.796	1.3464	1101	0.178	TiO_2	112	69.826
52	70.420	1.3360	2121	0.561	Al_2O_3	125	70.365
					$BaTiO_3$	212, 221	70.457
53					$Ba_2Ti_9O_{20}$		71.446
54	75.108	1.2638	5165	0.479	$BaTiO_3$	301, 310	75.143
55	76.882	1.2390	850	0.146	Al_2O_3	1.0.10	76.868
56					$BaTi_4O_9$	330	78.001
57	78.768	1.2140	495	0.278	$BaTiO_3$	113	78.799
					$BaTi_4O_9$		78.915
58	79.401	1.2059	2909	0.728	$BaTiO_3$	311	79.488
59	80.703	1.1897	841	0.443	$BaTi_4O_9$		80.637
					Al_2O_3	220	80.752
60	82.352	1.1700	504	0.186	TiO_2	321	82.387
61	83.501	1.1568	2066	0.406	$BaTi_4O_9$		83.333
					$BaTiO_3$	222	83.448
62	89.547	1.0937	696	0.129	TiO_2	222	89.506
63	90.762	1.0822	535	0.193	Al_2O_3	0.0.12	90.663
					TiO_2	330	90.633
64	92.049	1.0704	4434	0.438	$BaTiO_3$	312	92.149
65	92.238	1.0687	1228	0.310	$BaTiO_3$	312, 321	92.210
66	95.275	1.0425	1513	0.265	Al_2O_3	226	95.372
					TiO_2	411	95.372
67	96.017	1.0364	578	0.173	TiO_2	312	96.030

Table 5h: Results of IDR Peak Search for Sample S06D

Peak	2θ(deg)	d-spacing	Intensity	FWHM	Phase	hkl	2θ(deg)
1	18.635	4.7576	523	0.187	$BaTi_4O_9$	021	18.619
2	19.063	4.6519	978	0.173	$Ba_4Ti_{13}O_{30}$	102, 131	19.066
3	20.797	4.2677	2579	0.201	$Ba_4Ti_{13}O_{30}$	022, 040	20.769
4	22.052	4.0276	8838	0.434	$Ba_4Ti_{13}O_{30}$	231	22.026
					$BaTiO_3$	001, 100	22.208
5	23.146	3.8397	1068	0.177	$BaTi_4O_9$	031	23.197
6	25.590	3.4782	5059	0.242	Al_2O_3	210	25.545
7	26.222	3.3958	987	0.184	$Ba_4Ti_{13}O_{30}$	302	26.178
					$Ba_2Ti_9O_{20}$	411	26.269
8	27.446	3.2471	16566	0.186	$Ba_4Ti_{13}O_{30}$	110	27.448
					TiO_2		27.448
9	28.342	3.1464	7903	0.227	$Ba_4Ti_{13}O_{30}$	322, 113	28.267
					$BaTi_4O_9$	002 ,041	28.358
					$Ba_2Ti_9O_{20}$	130, 121	28.449
10	29.901	2.9858	1513	0.153	$BaTi_4O_9$		30.000
					$Ba_2Ti_9O_{20}$		30.000
11	30.464	2.9319	1039	0.168	$Ba_4Ti_{13}O_{30}$	213, 242	30.457
12	31.546	2.8338	36605	0.359	$BaTiO_3$	101, 110	31.506
13	32.040	2.7912	2776	0.219	$Ba_4Ti_{13}O_{30}$	133	32.015
14	33.000	2.7122	446	0.153	$Ba_2Ti_9O_{20}$	422, 440	32.015
					$Ba_4Ti_{13}O_{30}$		32.935
15	33.709	2.6567	3702	0.254	$Ba_2Ti_9O_{20}$		33.579
					$Ba_4Ti_{13}O_{30}$	313, 342	33.672
16	33.960	2.6377	1763	0.165	$Ba_4Ti_{13}O_{30}$	260	33.949
					$BaTi_4O_9$	032, 051	33.949
17	35.166	2.5499	6319	0.209	Al_2O_3	104	35.151
18	36.084	2.4871	5617	0.194	TiO_2	101	36.077
19	36.800	2.4404	437	0.185	$Ba_2Ti_9O_{20}$		36.635
					$Ba_4Ti_{13}O_{30}$	502, 531	36.728
20	37.798	2.3782	2921	0.229	Al_2O_3	110	37.752
21	38.909	2.3128	10690	0.325	$BaTiO_3$	111	38.874
					$BaTi_4O_9$	122, 150	39.062
22	40.199	2.2415	775	0.296	$Ba_4Ti_{13}O_{30}$	253, 271	40.186
					$Ba_2Ti_9O_{20}$	111	40.186
23	41.317	2.1834	5584	0.285	TiO_2	304, 362	41.222
					$Ba_4Ti_{13}O_{30}$		41.412
24	42.752	2.1134	672	0.240	$Ba_4Ti_{13}O_{30}$	602, 324	42.735
25	43.370	2.0847	6448	0.230	Al_2O_3	113	43.400
26	44.070	2.0532	1422	0.227	$Ba_4Ti_{13}O_{30}$	640	44.065
					TiO_2	210	44.065
27	44.964	2.0144	6240	0.353	$BaTiO_3$	002	44.828
					$Ba_4Ti_{13}O_{30}$	404, 462	44.924
					$BaTi_4O_9$	533	45.019
28	45.366	1.9975	7459	0.352	$Ba_4Ti_{13}O_{30}$	200	45.306
					$BaTiO_3$		45.402
29	46.197	1.9635	793	0.275	Al_2O_3	202	46.169
					$Ba_4Ti_{13}O_{30}$	471, 711	46.264
30	46.776	1.9405	1125	0.231	$Ba_4Ti_{13}O_{30}$	115, 173	46.746
31	47.267	1.9215	468	0.287	$BaTi_4O_9$		47.225
					$Ba_2Ti_9O_{20}$		47.225
32	47.891	1.8979	1275	0.222	$Ba_4Ti_{13}O_{30}$	642	47.902
					$BaTi_4O_9$	504, 562	47.999
33	49.108	1.8537	2108	0.298	$BaTi_4O_9$	235, 291	48.967
					$Ba_4Ti_{13}O_{30}$	102	49.062
34	50.155	1.8174	489	0.214	$Ba_2Ti_9O_{20}$	201	50.035
35	50.689	1.7995	1026	0.313	$Ba_4Ti_{13}O_{30}$		50.620
					$BaTiO_3$		50.620
36	50.880	1.7932	2459	0.447	$BaTiO_3$	202	51.011
37	52.569	1.7395	3311	0.276	Al_2O_3	544, 604	52.582
38	53.864	1.7007	430	0.139	$Ba_4Ti_{13}O_{30}$		53.963
					$BaTi_4O_9$		54.063

Table 5h: Results of IDR Peak Search for Sample S06D (cont.)

39	54.348	1.6867	8236	0.242	$Ba_2Ti_9O_{20}$		54.260
					TiO_2	211	54.361
40	56.257	1.6339	11285	0.467	$BaTiO_3$	211	56.253
41	56.642	1.6237	2399	0.181	TiO_2	220	56.653
					$BaTi_4O_9$		56.756
42	57.515	1.6011	6927	0.275	Al_2O_3	116	57.559
					$Ba_2Ti_9O_{20}$		57.559
43	58.135	1.5855	409	0.205	$BaTi_4O_9$	644	58.264
44	58.609	1.5738	432	0.222	$Ba_4Ti_{13}O_{30}$		58.467
					$BaTi_4O_9$		58.769
45	59.313	1.5568	570	0.136	$Ba_4Ti_{13}O_{30}$	704, 762	59.279
46	60.696	1.5246	536	0.211	$Ba_2Ti_9O_{20}$		60.806
47	61.314	1.5107	579	0.235	Al_2O_3	122, 018	61.274
48	61.950	1.4967	497	0.195	$BaTi_4O_9$		61.936
49	62.775	1.4790	1021	0.244	TiO_2	002	62.761
50	64.065	1.4523	660	0.147	$BaTi_4O_9$		64.006
					TiO_2	210	64.006
51	65.176	1.4302	689	0.270	$Ba_2Ti_9O_{20}$		65.366
52	65.902	1.4162	5473	0.621	$BaTiO_3$	202, 220	65.930
					$Ba_2Ti_9O_{20}$		65.996
53	66.511	1.4047	2822	0.284	Al_2O_3	124	66.522
54	68.226	1.3735	4370	0.243	Al_2O_3	030	68.221
55	69.028	1.3595	1525	0.162	TiO_2	301	68.970
56	69.796	1.3464	908	0.158	TiO_2	112	69.826
57	70.438	1.3357	1167	0.419	Al_2O_3	125	70.365
					$BaTiO_3$	212, 221	70.457
58					$Ba_2Ti_9O_{20}$		71.446
59	75.094	1.2640	2216	0.491	$BaTiO_3$	301, 310	75.143
60	76.882	1.2390	688	0.173	Al_2O_3	1.0.10	76.868
61					$BaTi_4O_9$	330	78.001
62	82.344	1.1701	1178	0.260	TiO_2	321	82.387
63	83.492	1.1569	1611	0.434	$BaTi_4O_9$		83.333
					$BaTiO_3$	222	83.448
64	86.349	1.1258	369	0.259	Al_2O_3	312	86.321
65	89.021	1.0988	595	0.316	Al_2O_3	0.2.10	89.134
66	89.547	1.0937	655	0.158	TiO_2	222	89.506
67	90.740	1.0824	569	0.151	Al_2O_3	0.0.12	90.663
					TiO_2	330	90.633
68	92.205	1.0690	2342	0.381	$BaTiO_3$	312, 321	92.210
69	95.263	1.0426	1319	0.231	Al_2O_3	226	95.372
					TiO_2	411	95.372
70	95.993	1.0366	489	0.183	TiO_2	312	96.030

Table 6: Intensity Data for Selected Peaks

Sample	Al_2O_3 110	Al_2O_3 024	Al_2O_3 SUM	TiO_2 101	TiO_2 102	TiO_2 SUM	$BaTiO_3$ 213	$BaTi_4O_9$ 031	$Ba_4Ti_{13}O_{30}$ 022,040
Sraw	381	521	901	1491	276	1767	1939	0	0
S24M	391	508	900	1352	243	1595	1971	52	17
S01H	393	492	886	1369	245	1614	1835	65	19
S02H	431	541	972	1267	241	1509	1856	102	34
S08H	409	538	947	1117	207	1323	1680	127	118
S24H	436	516	952	1109	197	1306	1389	148	170
S48H	469	568	1036	1011	180	1191	1319	175	268
S06D	461	543	1004	915	119	1033	1012	170	417
k_i						1.53	2.01		

Table 7: Results of Phase Identification and Quantitative Analysis

Time (hours)	Wt % $BaTiO_3$	Wt % Int. Phases	Wt % $Ba_6Ti_{17}O_{40}$	Wt % $Ba_4Ti_{13}O_{30}$	Wt % $BaTi_4O_9$	Wt % $Ba_2Ti_9O_{20}$	Wt % TiO_2
0	0.455	0.000	--	--	--	--	0.545
0.4	0.467	0.035	X	***	***	X	0.498
1	0.442	0.046	X	***	***	X	0.512
2	0.408	0.156	X	***	***	X	0.436
8	0.378	0.229	X	***	***	***	0.392
24	0.311	0.305	X	***	***	***	0.385
48	0.271	0.406	X	***	***	***	0.323
144	0.215	0.496	X	***	***	***	0.289

Table 8: Data for the $BaCO_3$ - TiO_2 Reaction

Equimolar $BaCO_3$ - TiO_2 Mixture Heated at 1050°C in Air

Time (hours)	Mole % $BaCO_3$	Mole % Ba_2TiO_4	Mole % $BaTiO_3$	Mole % $Ba_4Ti_{13}O_{30}$	Mole % $BaTi_4O_9$	Mole % TiO_2
0	50	--	--	--	--	50
0.25	13	41	12	6	1?	28
0.50	5	51	17	4	1?	23
1.0	0	48	30	4	1?	17
2.0	0	44	37	4	1?	14

From Templeton and Pask[4]

Notes:

1. $Ba_4Ti_{13}O_{30}$ reported as $BaTi_3O_7$.
2. Detectability of $BaTi_4O_9$ a nd $Ba_4Ti_{13}O_{30}$ reported as 2-3 mole %.

Figure 1a

Simplified $BaCO_3$ - TiO_2 Interface Reactions

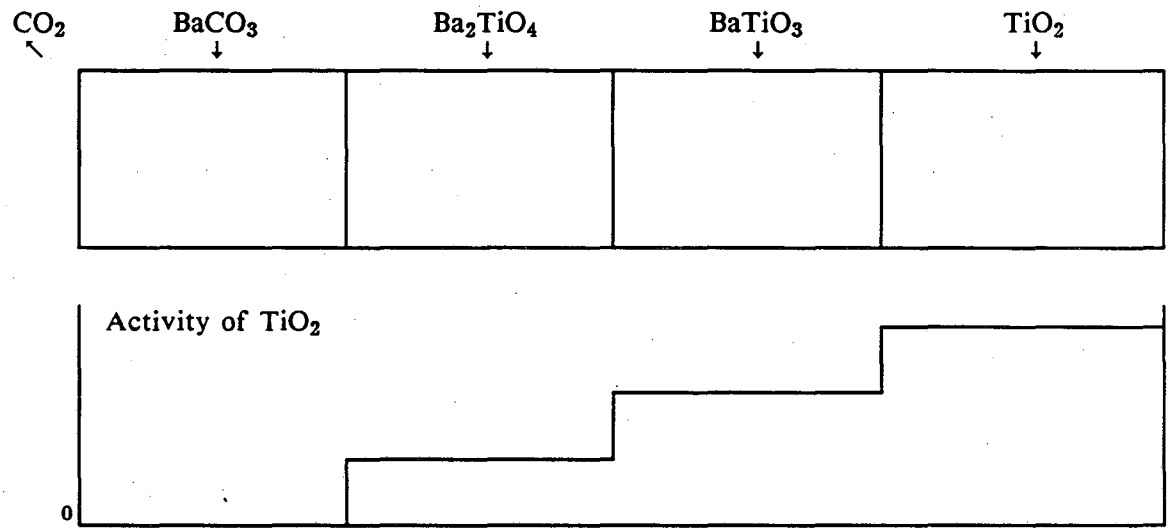

Figure 1b

Complex $BaCO_3$ - TiO_2 Interface Reactions

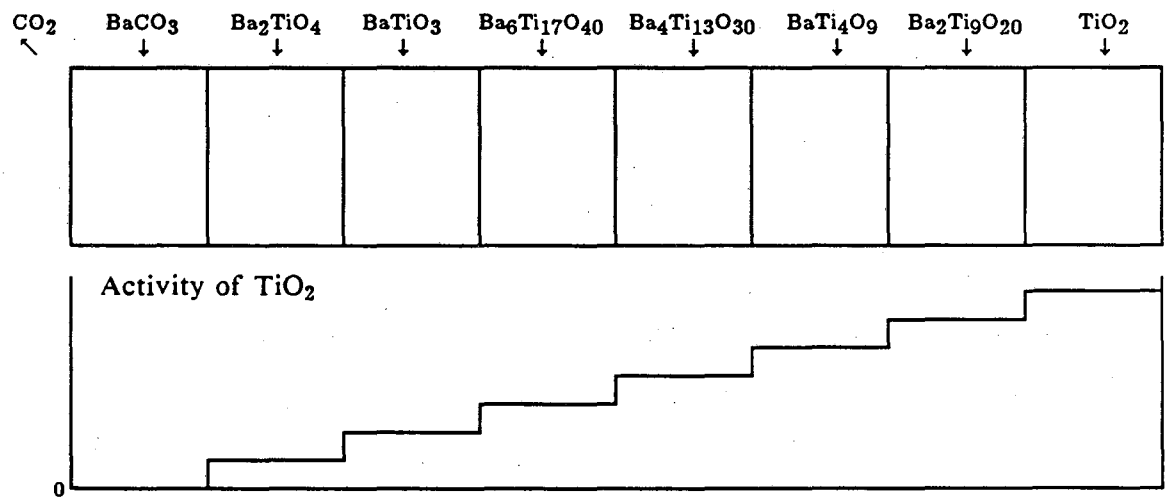

Figure 2
BaO - TiO_2 Phase Diagram

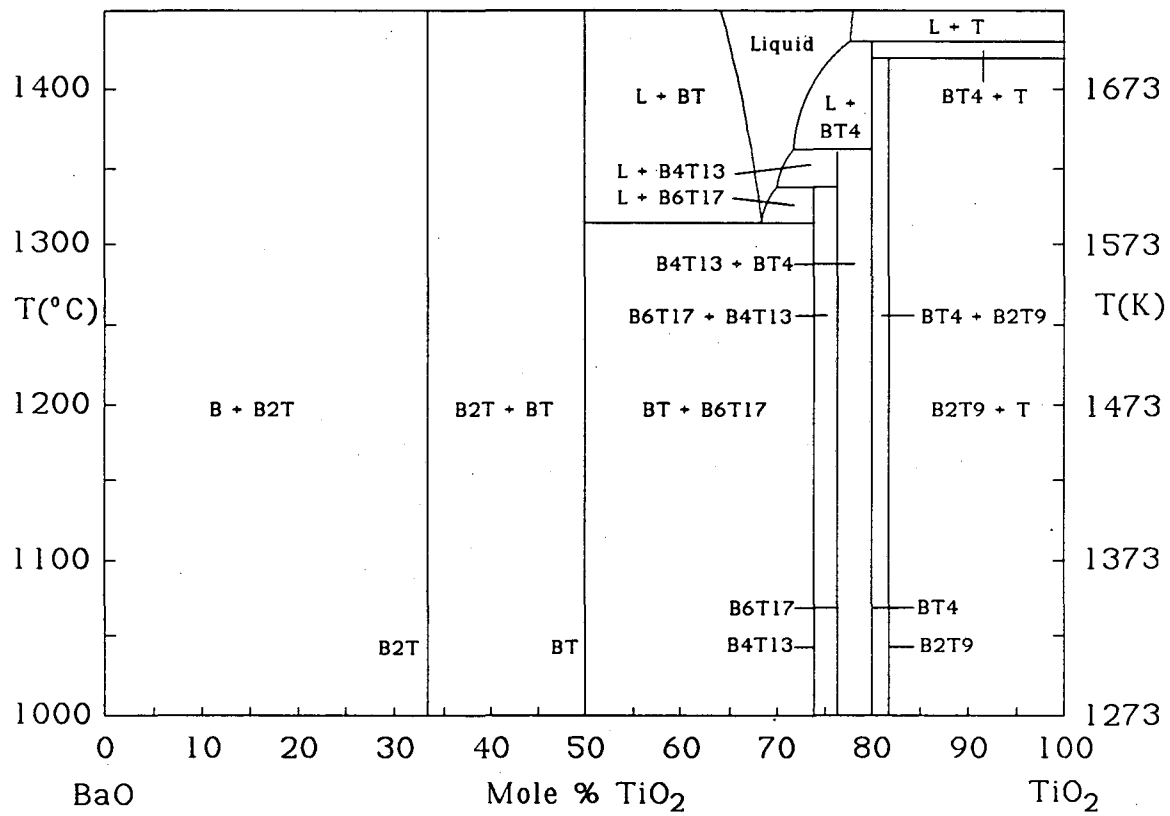

Key:
L=Liquid; B=BaO; B2T=Ba_2TiO_4; BT=$BaTiO_3$; B6T17=$Ba_6Ti_{17}O_{40}$;
B4T13=$Ba_4Ti_{13}O_{30}$; BT4=$BaTi_4O_9$; B2T9=$Ba_2Ti_9O_{20}$; T=TiO_2;

References:

1. W. Trzebiatowski, M. Drys, and J. Berak, *Roczniki Chemii* **28** 21-28 (1954)
2. D. E. Rase, R. Roy, *J. Amer. Cer. Soc.* **38**(3) 102-113 (1955)
3. T. Negas, R.S. Roth, H.S. Parker, and D. Minor, *J. Sol. State Chem.* **9** 297-307 (1974)
4. H.M. O'Bryan, Jr., and J. Thomson, *J. Amer. Cer. Soc.* **57**(12) 522-526 (1974)

Figure 3
Possible Geometric Arrangement of Product Phases During Solid State Reaction

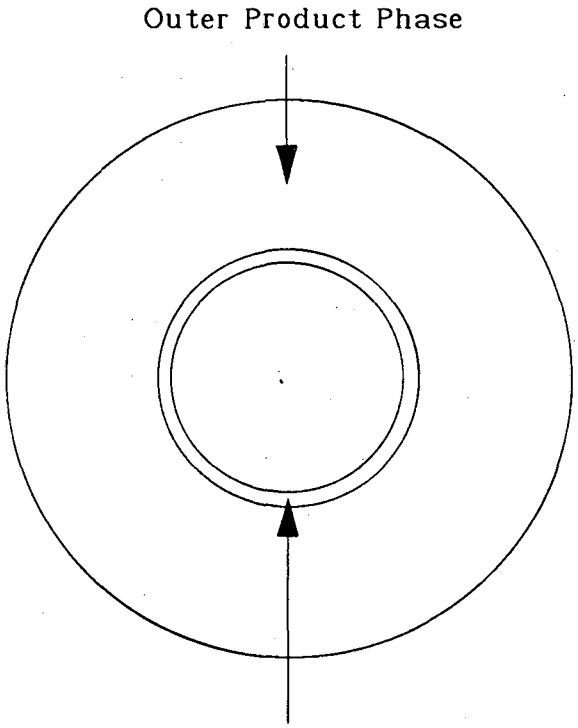

Figure 4
X-ray Diffraction Patterns of Starting Materials

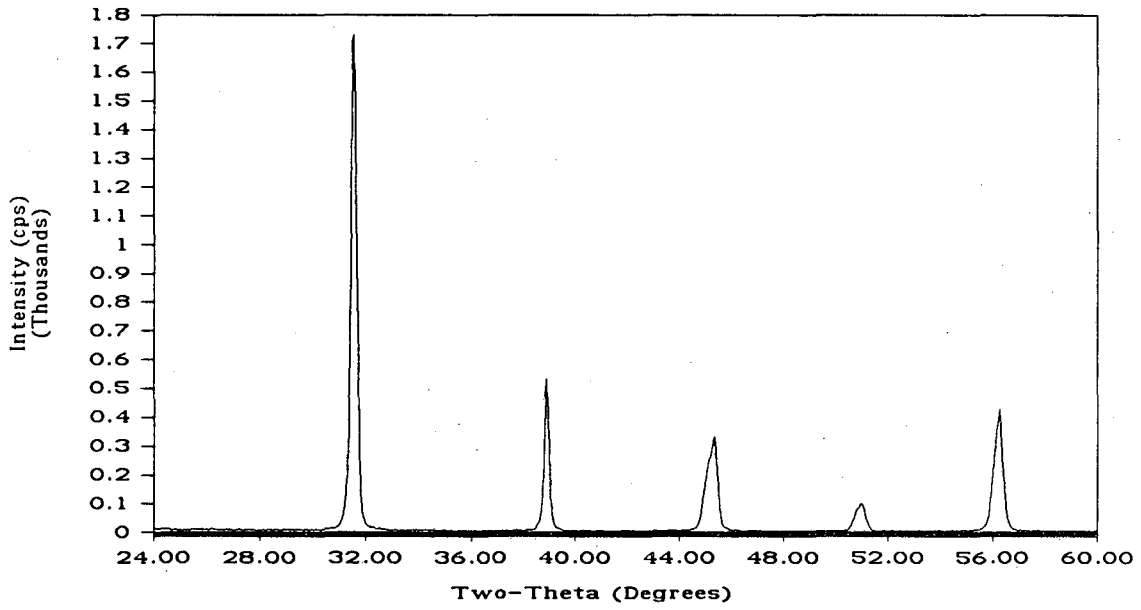

a. $BaTiO_3$

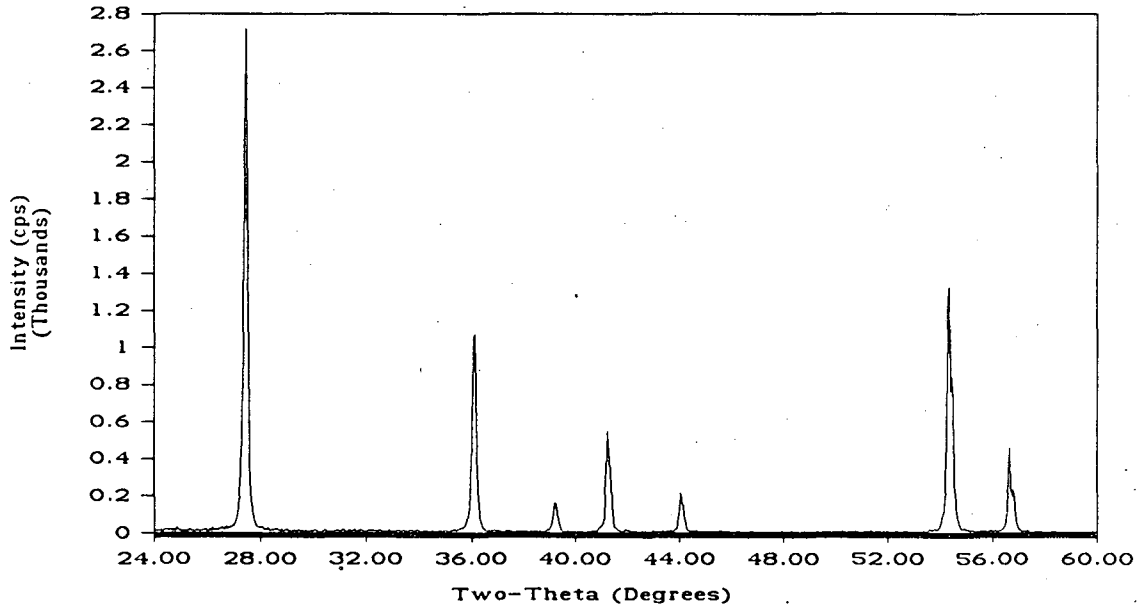

b. TiO_2

Figure 4 (continued)

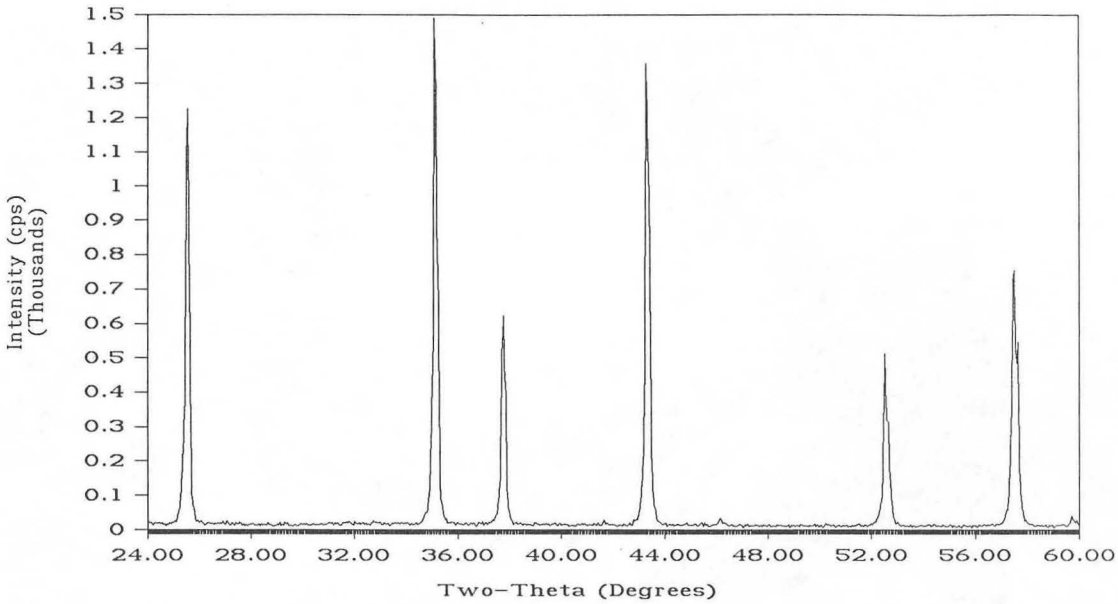

c. Al_2O_3

Figure 5
SEM Micrographs of Starting Materials

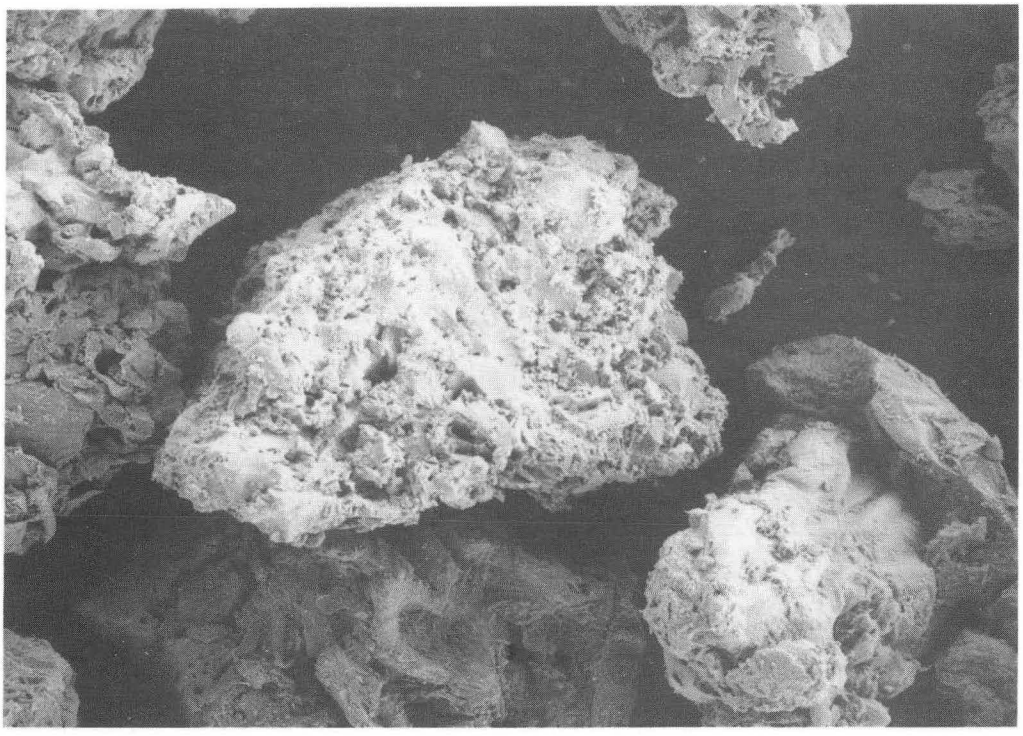

a. $BaTiO_3$ 1000× —— 10.0μm

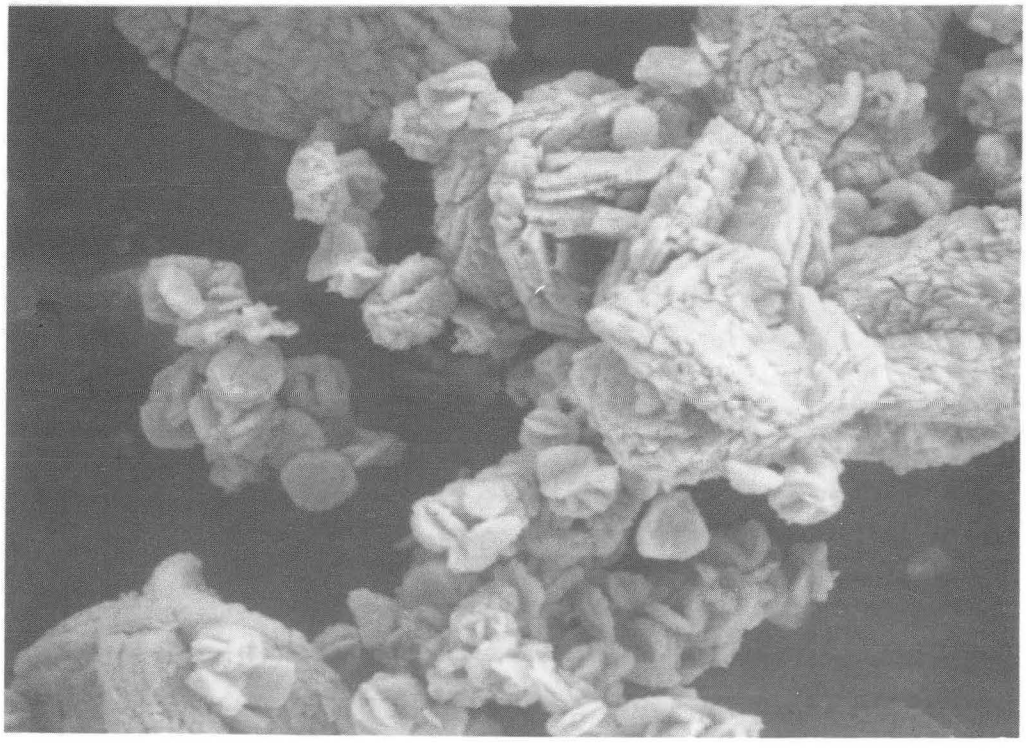

b. TiO_2 77× —— 130μm

XBB 885-4850

Figure 6
SEM Micrograph of Unfired Mixed Powder

126× —— 79.4μm

XBB 885-4851

Figure 7
SEM Micrograph of Sample S06D

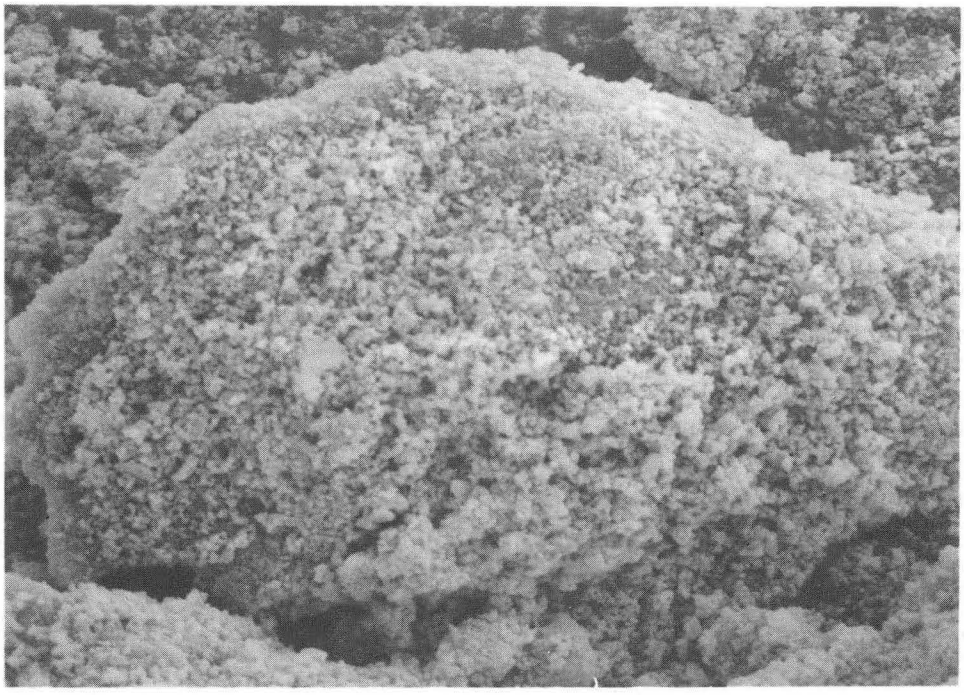

2400× —— 4.17μm

Figure 8
SEM Micrograph of Sample S08H

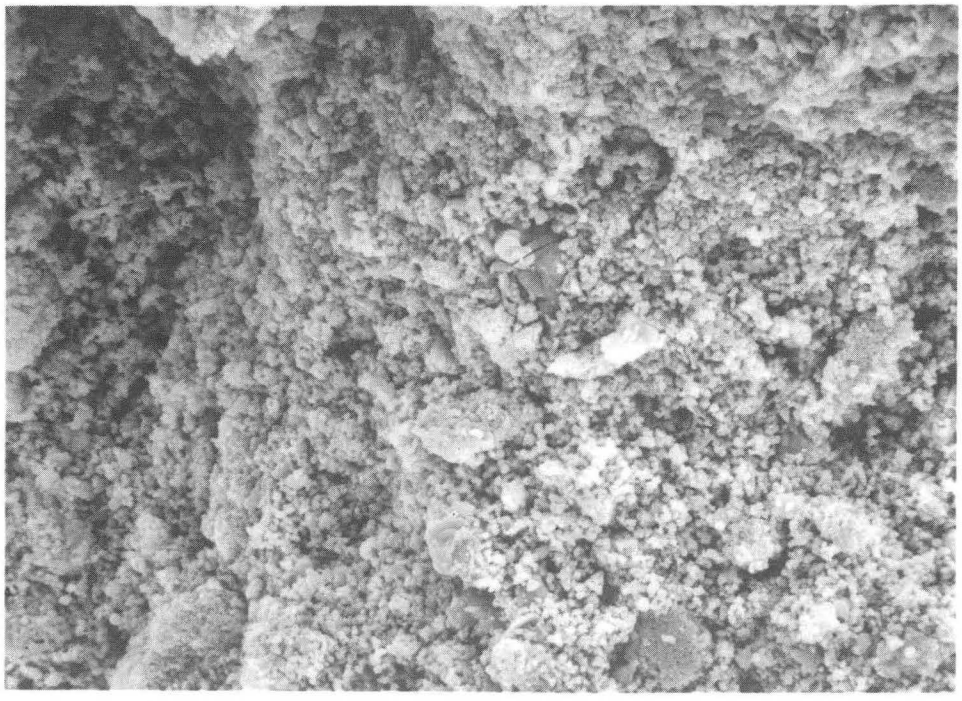

2240× —— 4.46μm

XBB 885-4852

Figure 9a
Xray Diffraction Patterns for All Samples

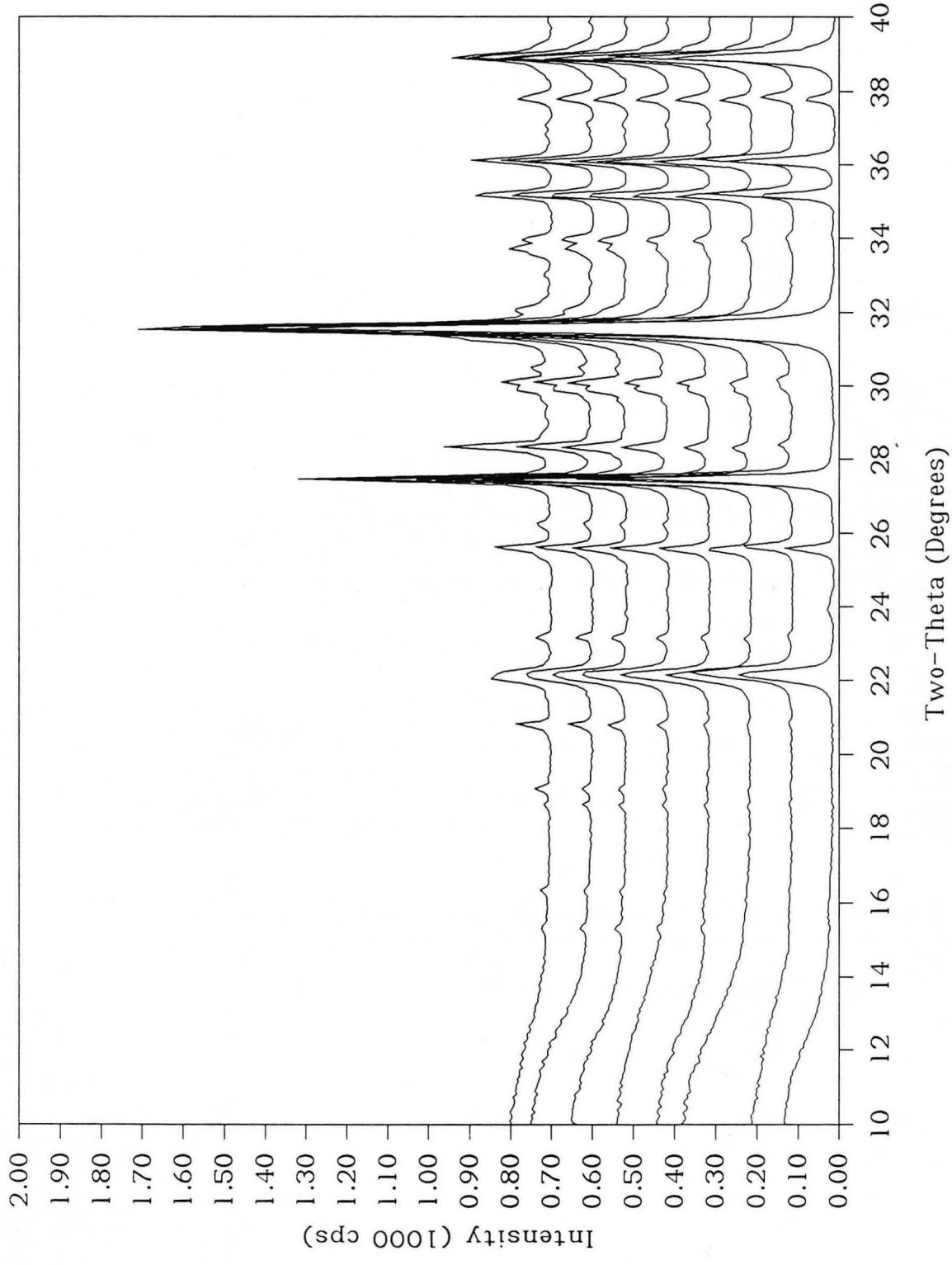

Figure 9b
Xray Diffraction Patterns for All Samples

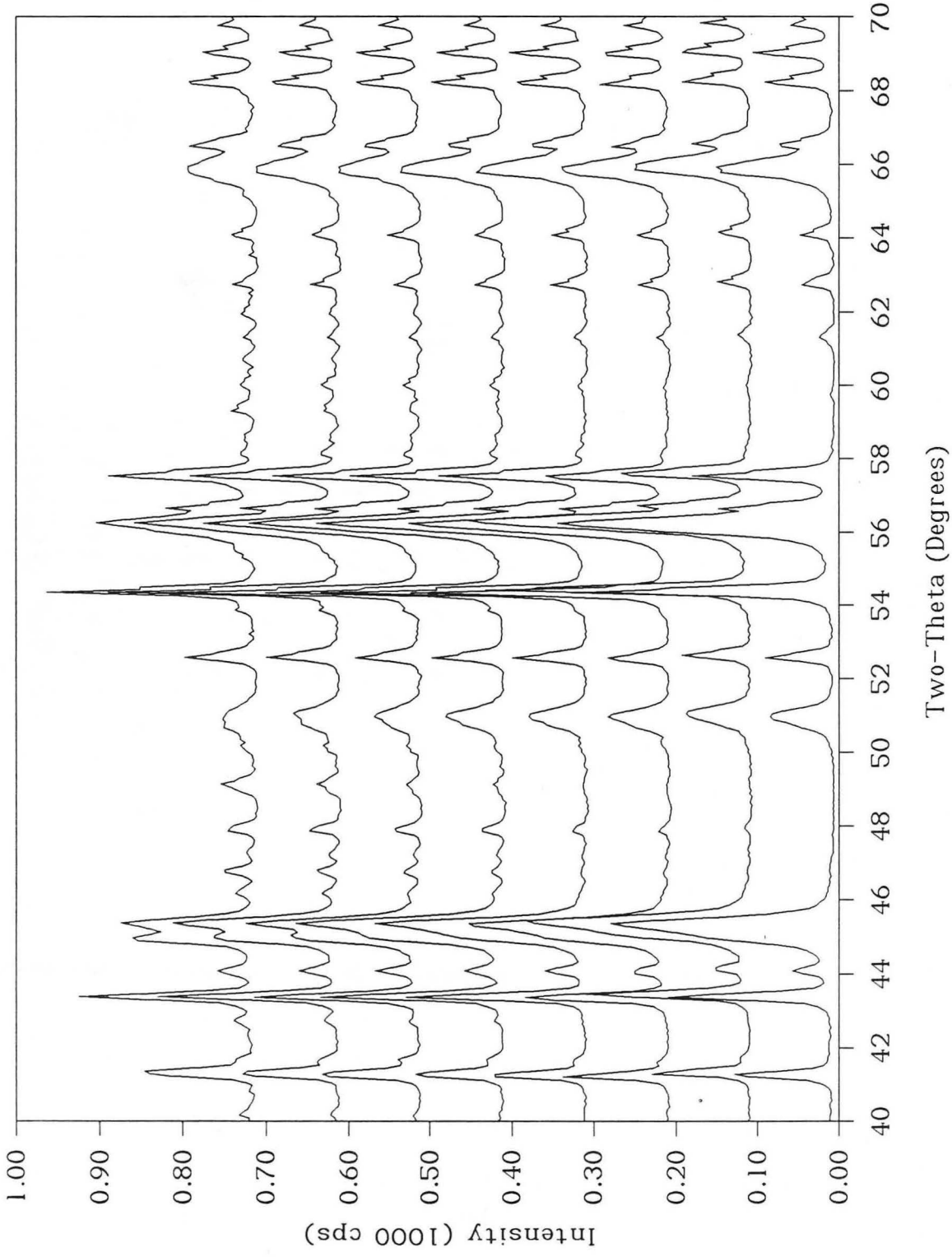

Figure 9c
Xray Diffraction Patterns for All Samples

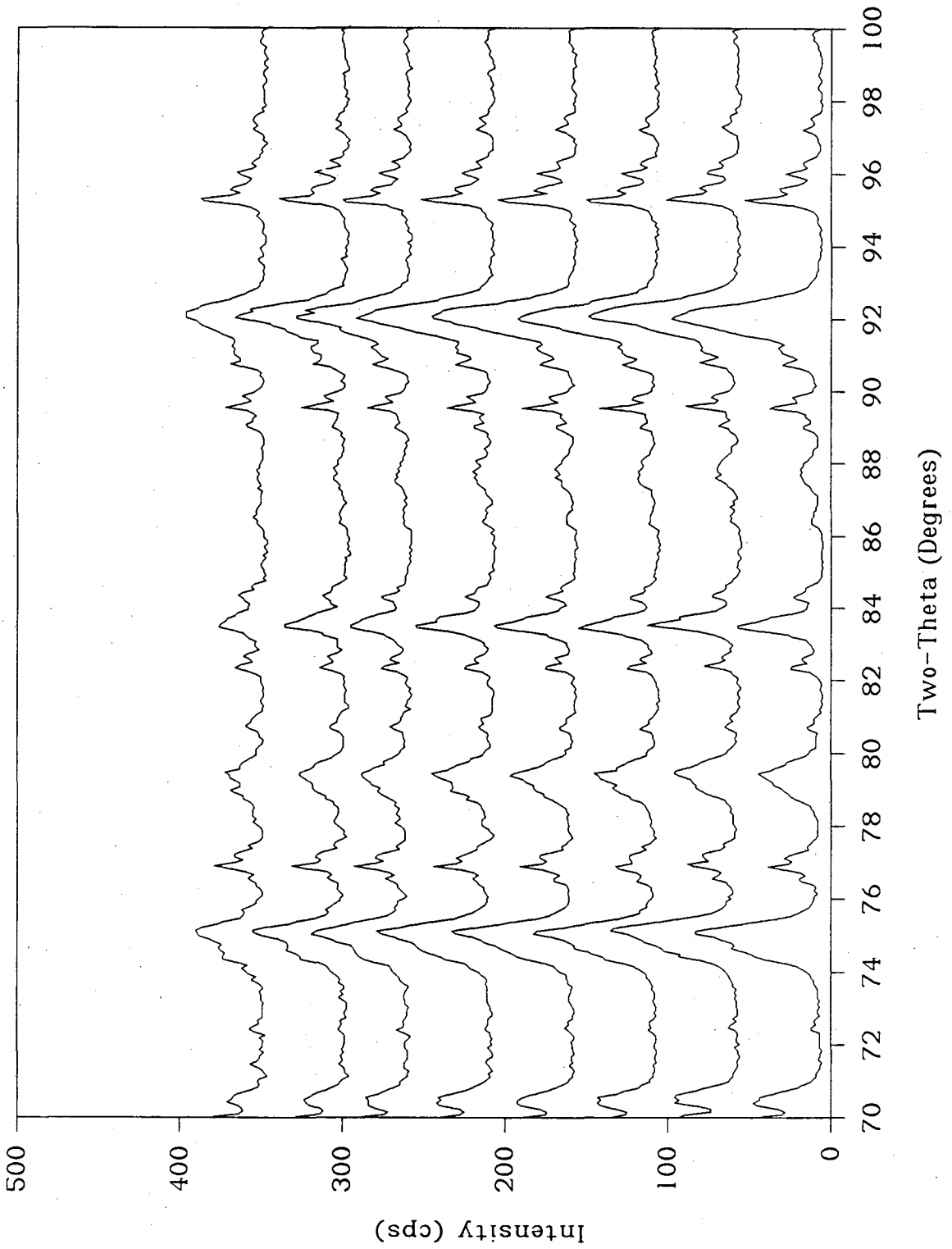

Figure 10
Xray Diffraction Pattern Showing the Calculation of Background Lines

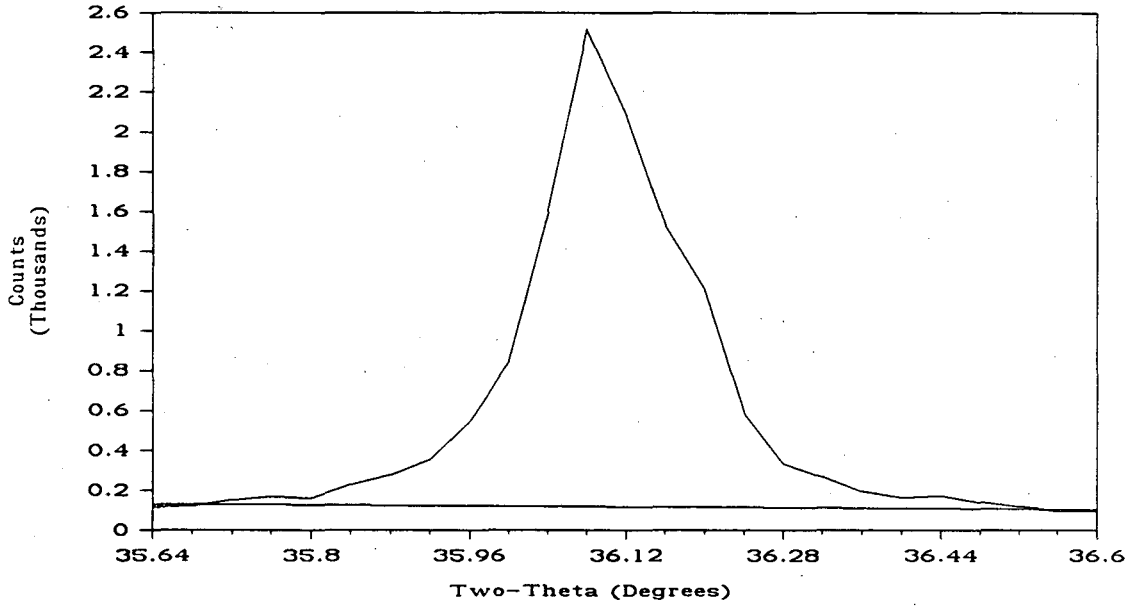

a. 101 Peak of TiO_2 - Sample S24M

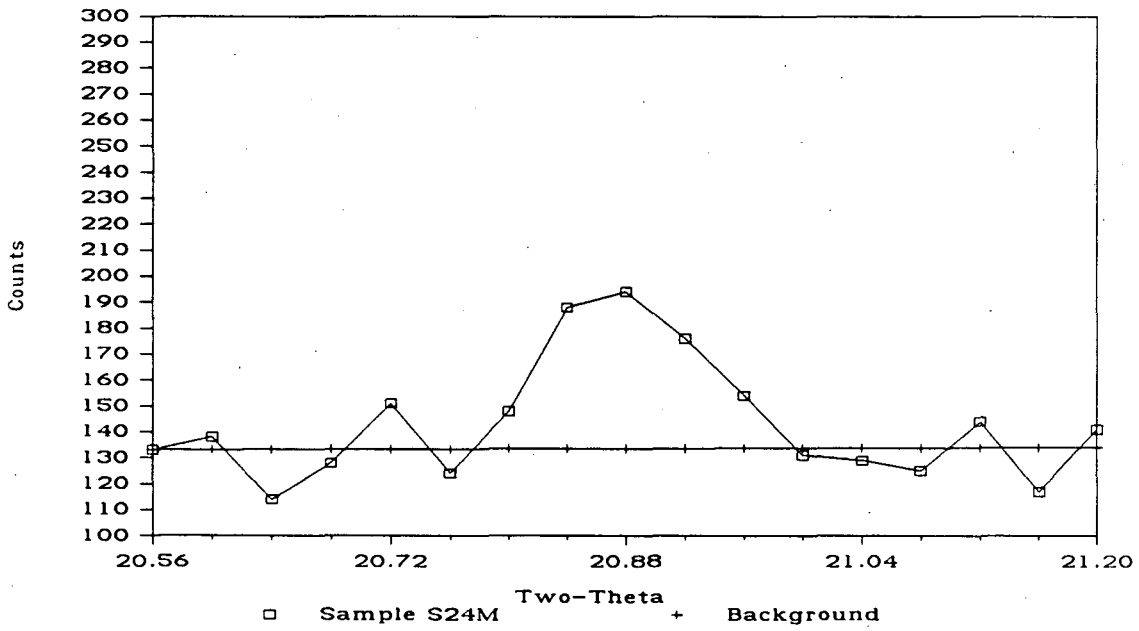

b. 022,040 Peak of $Ba_4Ti_{13}O_{40}$ - Sample S24M

Figure 11
Xray Diffraction Patterns for the 031 Peak of $BaTi_4O_9$

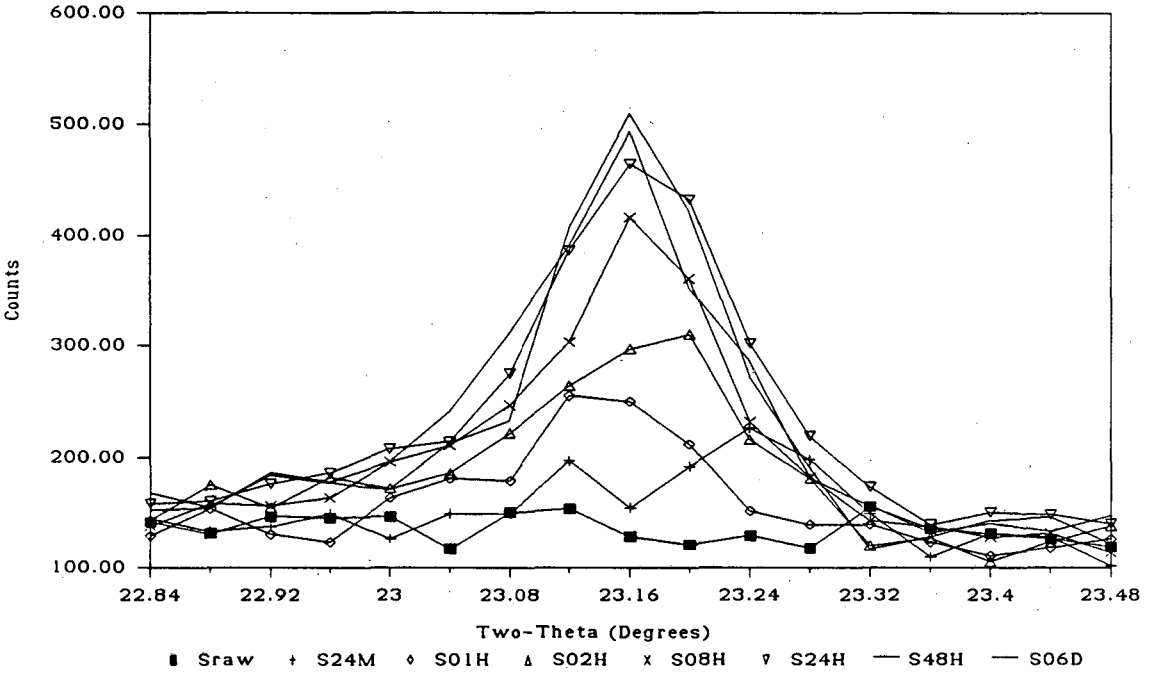

Figure 12
Xray Diffraction Patterns for the 022,040 Peak of $Ba_4Ti_{13}O_{30}$

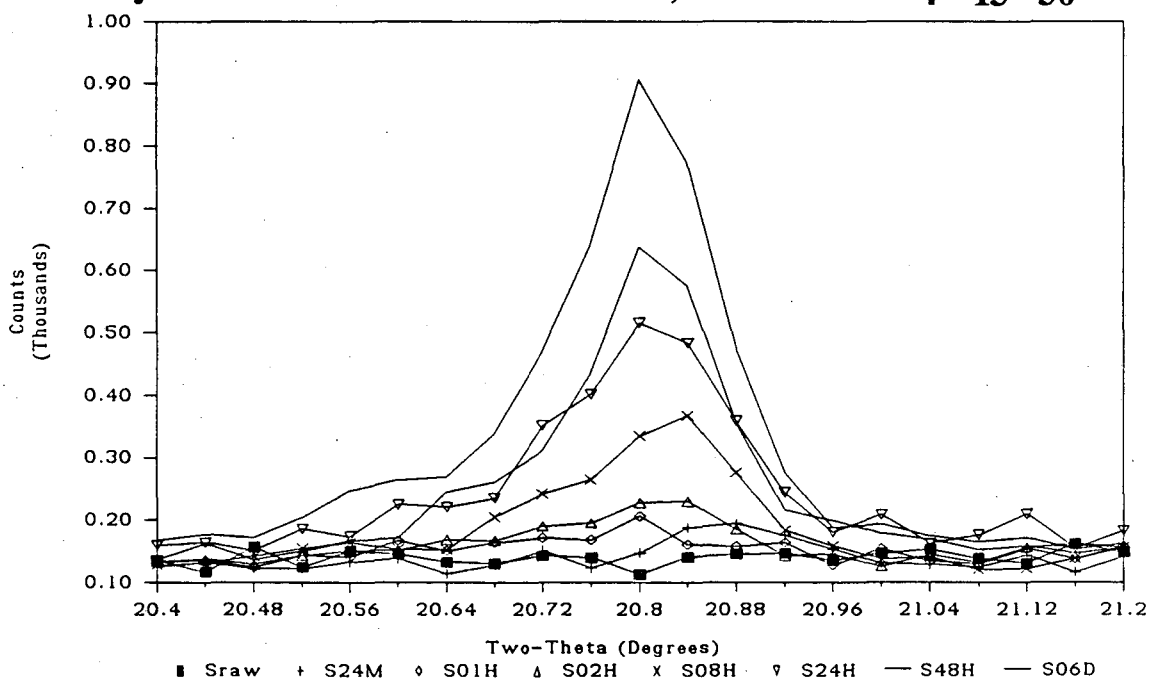

Figure 13
Xray Diffraction Patterns for the 021 Peak of $BaTi_4O_9$ and the 102,131 Peak of $Ba_4Ti_{13}O_{30}$

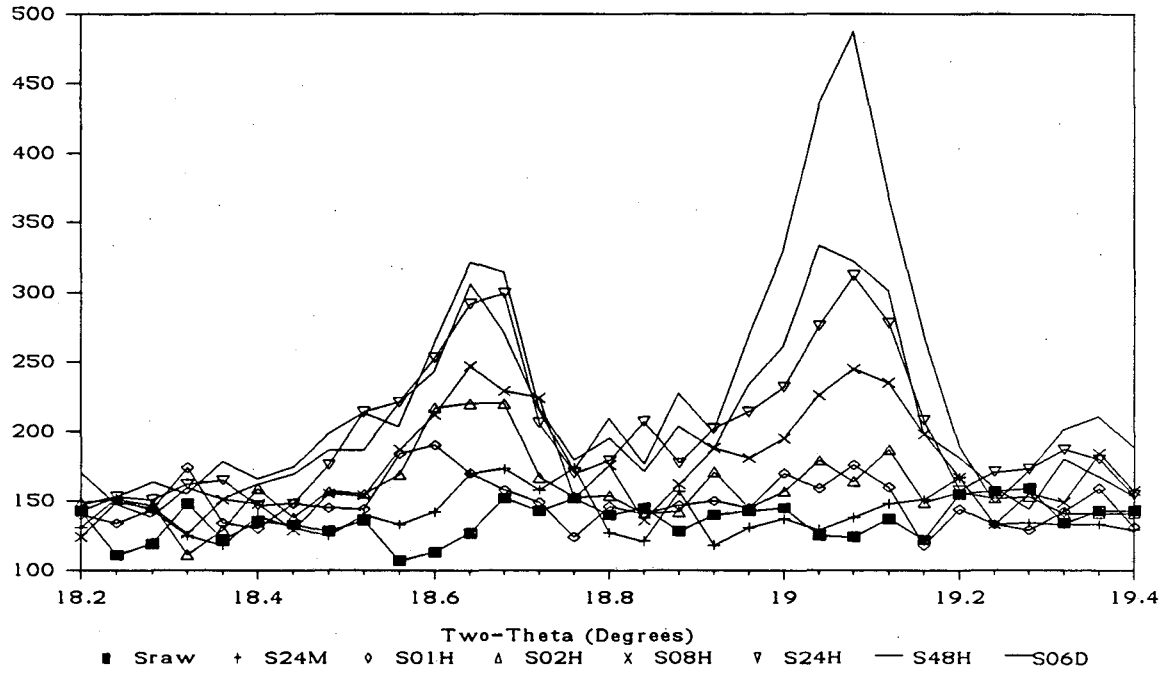

Figure 14
Xray Diffraction Patterns for the Selected Peaks of $Ba_2Ti_9O_{20}$

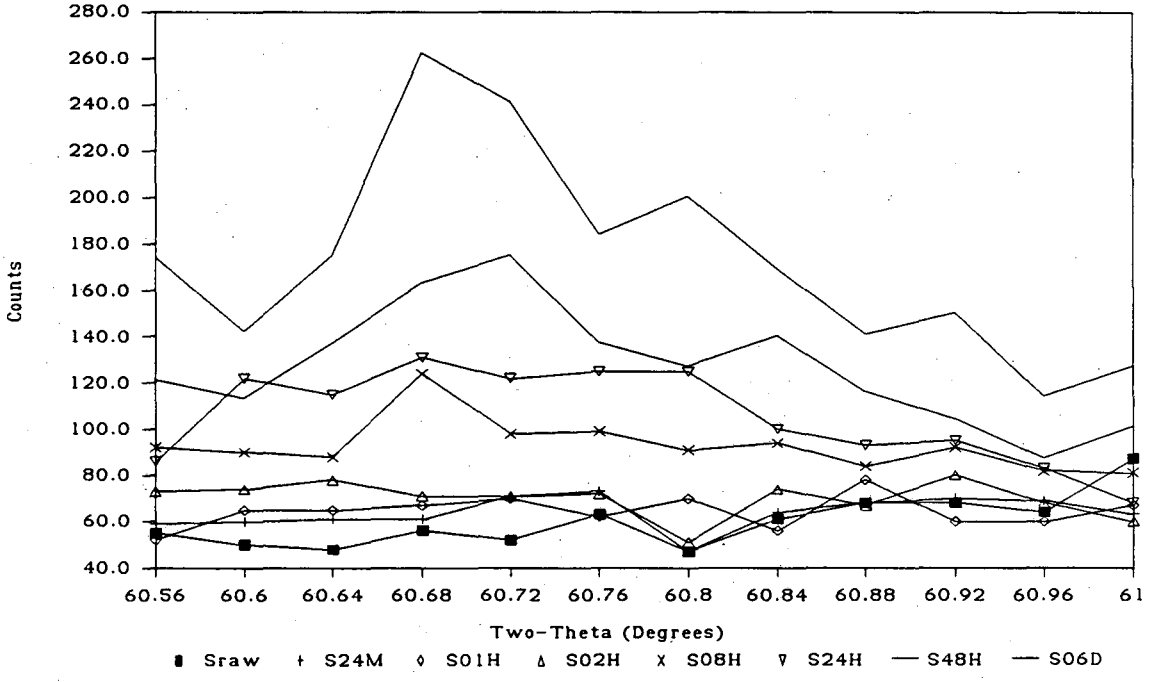

a. Peak at 60.806° (60.68°)

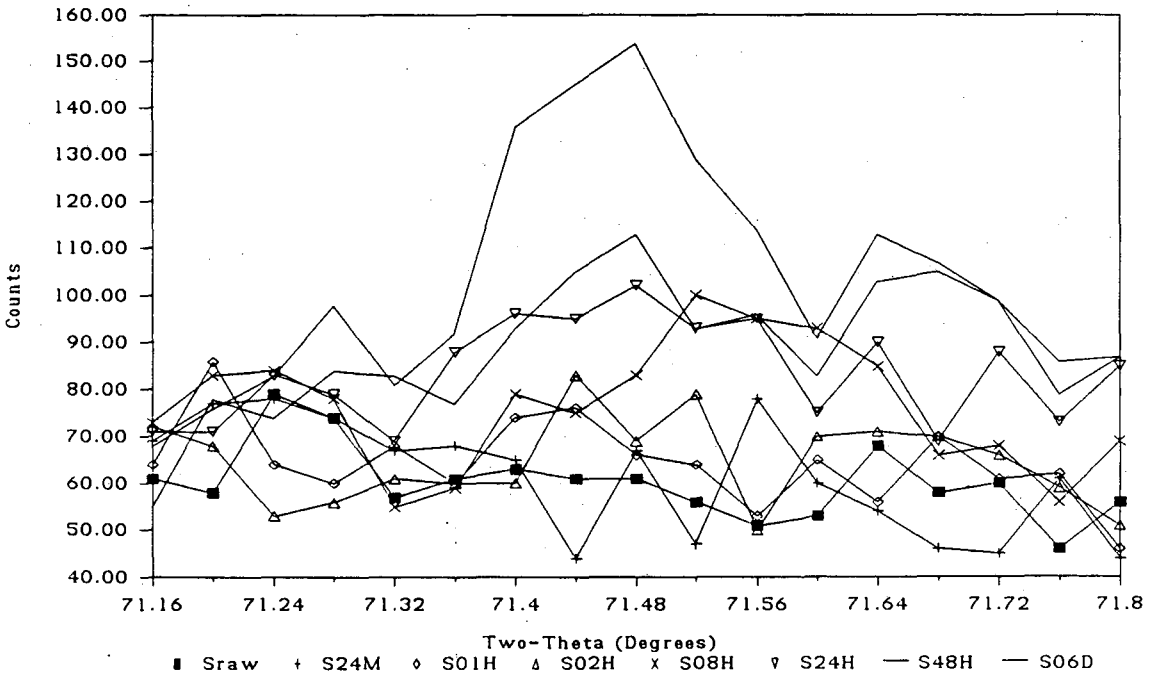

b. Peak at 71.446°

Figure 15
Weight Fraction of TiO_2, $BaTiO_3$, and Total Amount of Intermediate Phases with Time

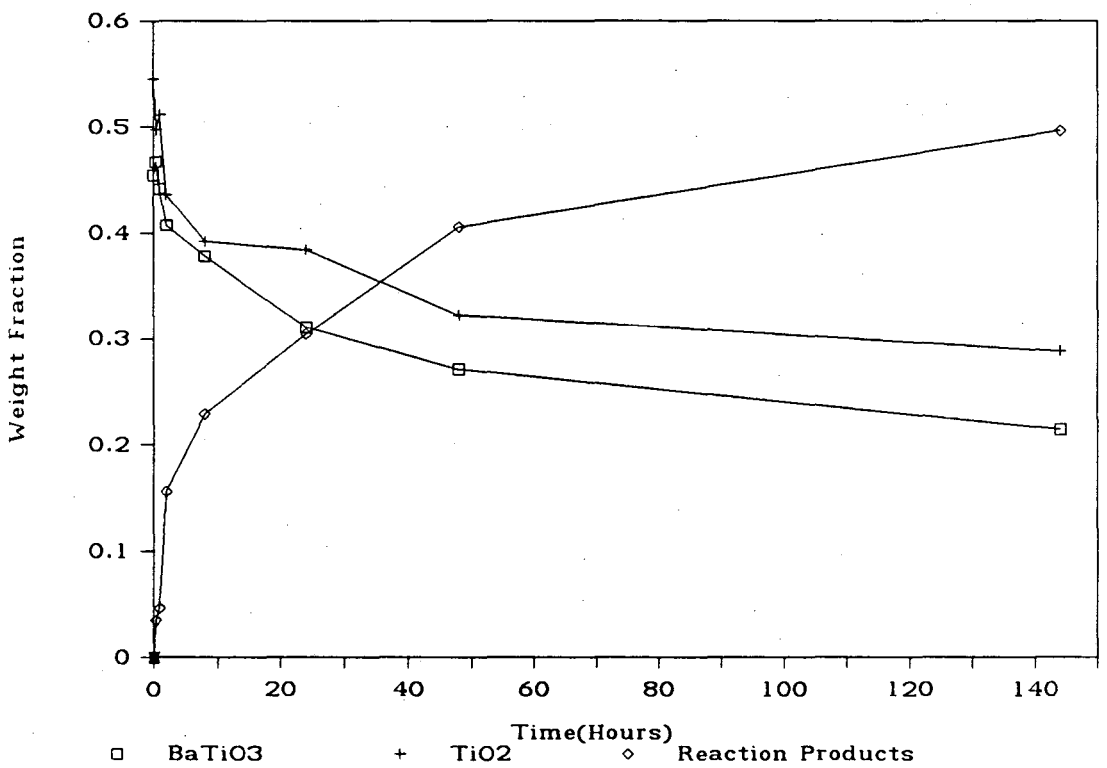

Figure 16
Normalized Intensity of Observed Intermediate Phases with Time

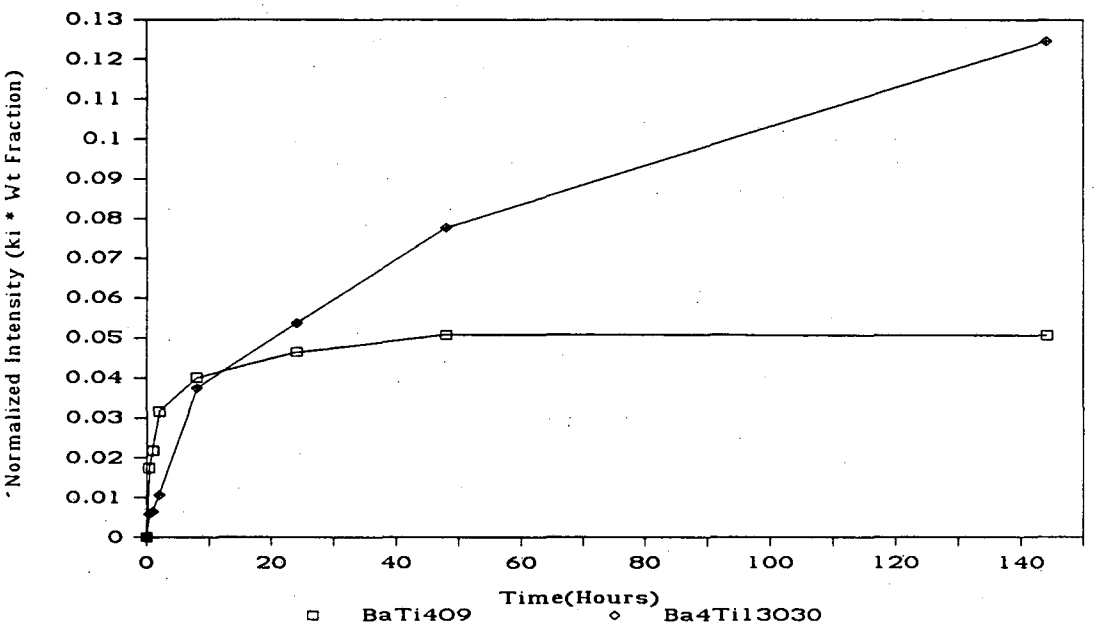

Figure 17
Normalized Intensity of Observed Intermediate Phases with Square Root of Time

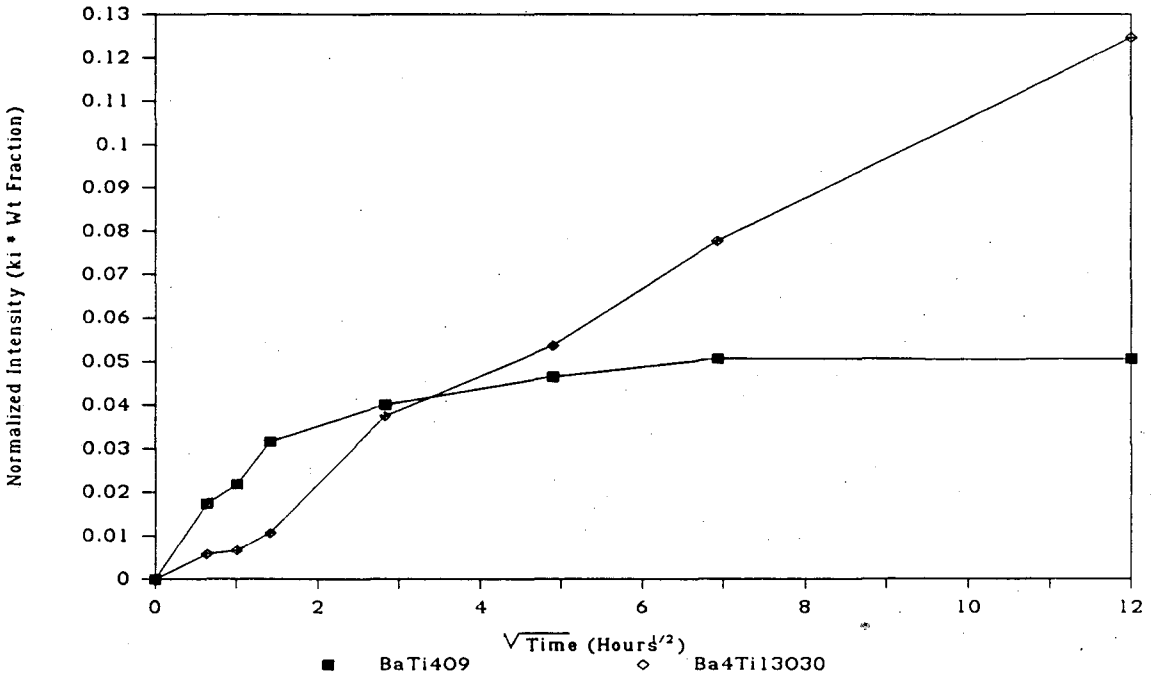

LAWRENCE BERKELEY LABORATORY
TECHNICAL INFORMATION DEPARTMENT
1 CYCLOTRON ROAD
BERKELEY, CALIFORNIA 94720